Necromass chemistry interacts with soil mineral and microbial properties to determine fungal carbon and nitrogen persistence in soils

Katilyn V. Beidler[1,2*], Elizabeth Huenupi [1], Lang C. DeLancey[3], François Maillard[4], Bowen Zhang[5], Per Persson[4,5], Peter G. Kennedy[2] & Richard Phillips[1]

1. Department of Biology, Indiana University, Bloomington, IN, 47405 , United States of America
2. Department of Plant and Microbial Biology, University of Minnesota, St. Paul, MN, 55108, United States of America
3. Ecology, Evolution, and Behavior Graduate Program, University of Minnesota, St. Paul, MN, 55108, United States of America
4. Department of Biology, Microbial Ecology Group, Lund University, Sölvegatan 35, SE-22362, Lund, Sweden
5. Centre for Environmental and Climate Science, Faculty of Science, Lund University, Ecology Building, Sölvegatan 37, SE-22362, Lund, Sweden

*Corresponding Author
Katilyn V. Beidler
beidl006@umn.edu
1030 Manvel Street,
Saint Paul MN 55114
843-830-4679

Keywords: Melanin, Mineral-associated soil organic matter, Iron oxide, Potentiometric titration

Abstract

Despite fungal necromass being increasingly recognized a major source of carbon (C) and nitrogen (N) in soils, understanding of how soil mineral and microbial properties interact with initial necromass chemistry to influence its accumulation and persistence remains limited. To track the fate of fungal C and N into mineral associated organic matter (MAOM), we generated dual-labeled ^{13}C and ^{15}N fungal necromass of high and low melanin phenotypes of *Hyaloscypha bicolor*. Necromass was incubated in live and sterile soils from six forests in Indiana, USA that differed in initial microbial and physiochemical characteristics. At the end of the 38-day incubation, considerably more initial fungal necromass N was incorporated into MAOM relative to necromass C and low melanin necromass contributed more to MAOM-C formation. Though soil iron oxide (FeOx) and clay content were positively correlated with MAOM-C formation from low melanin necromass, initial microbial community composition was the best predictor of MAOM-N formation for both high and low melanin necromass additions. In particular, soils with higher relative abundances of bacterial copiotrophs at the start of the study formed less fungal necromass-derived MAOM-N. We also used synthesized FeOx minerals to investigate how initial necromass chemistry impacts mineral sorption *in vitro*. We found higher adsorption of amide functionalities for low melanin necromass on goethite minerals after 24 hours. However, 30% less initial necromass-N was converted into MAOM-N in sterile soils regardless of necromass type. When considered together, our results indicate that the microbial synthesis pathway drives fungal necromass-derived MAOM-N formation and that microbial processing limits fungal necromass-derived MAOM-C formation, highlighting the importance of microbial controls on the preservation of fungal-derived SOM in soils.

Introduction

To reach sparse soil resources, it is estimated that fungi produce an average of one kilometer of hyphae per cubic centimeter of soil (See et al. 2022). High hyphal densities combined with rapid turnover make fungi major, if not the main microbial contributors to soil organic carbon (SOC) and nitrogen (SON; Godbold et al. 2006; Wang et al. 2021). An estimated 30-50% of soil C and 60-80% of soil N is microbial in origin (Simpson et al. 2007; Hu et al. 2020; Wang et al. 2021; Warren 2021), with dead fungal hyphae (hereafter fungal necromass) forming up to two-thirds of all microbial necromass (Liang et al. 2019; Wang et al. 2021). Though soil C and N accumulate slowly (on the scale of years to millennia), microbial compounds can stabilize in soil over relatively short timespans (days to months), because small, charged microbial compounds readily bind to active sites on clays and metal precipitates in soils (Kleber et al. 2007; Lützow et al. 2006; Cotrufo et al. 2013; Lehmann and Kleber 2015; Cotrufo and Lavallee 2022). These organo-mineral associations may persist over hundreds of years, as they are biologically, chemically, and physically protected from further decay (Sollins et al. 1996; Kögel-Knabner 2002; Kleber et al. 2015). Given the extensive presence of fungal hyphae in soils, their close proximity to soil minerals, and the unique chemical composition of fungal cells (Kögel-Knabner 2002; Godbold et al. 2006; See et al. 2022), it is important to identify the dominant ecological factors controlling fungal-derived SOM formation and persistence.

The soil mineral matrix or physicochemical context in which hyphae live and die dictates soil organic matter (SOM) formation (Lützow et al. 2006; Frey et al. 2019). Due to differences in parent material and weathering conditions, soils can vary greatly in their mineralogy and thus their capacity for binding SOM. Under similar climatic conditions, soil clay content correlates positively with SOC and percent clay is frequently used as a proxy variable for SOM pools in terrestrial C cycling models (Sulman et al. 2014; Bailey et al. 2018; Matus 2021). Together with clay sized particles, amorphous metal oxides provide the greatest surface area on which organic matter (OM) can bind (Lützow et al. 2006). Metal oxides may be better predictors of SOM persistence than clay content alone, as not all mineral surfaces are equal in their binding potential (Goldberg 1990; Rasmussen et al. 2018). Iron (hydro)oxides (FeOx) have high densities of reactive hydroxyl (-OH) sites and thus increased capacity for ligand exchange or -OH exchange between carboxyl or phenolic functional groups in OM and -OH functionalities on mineral surfaces (Harsh et al. 2018; Wu et al. 2023). Ligand exchange results in stronger bonds compared to OM-cation-mineral interactions (i.e., polyvalent cation bridges) and thus has increased capacity to stabilize OM (Lützow et al. 2006; Mikutta et al. 2007). However, the charge and reactivity of mineral constituents with

OM are ultimately dependent upon soil pH, which is considered a “master soil variable” (Deng and Dixon 2018; Rasmussen et al. 2018; Wang and Kuzyakov 2024). Furthermore, soil pH and mineralogy interact to have indirect effects on SOM dynamics by shaping microbial decomposer communities through the availability of oxygen, water, and nutrients in soil pores (Fierer and Schimel 2002; Kallenbach et al. 2016).

Fungal necromass supports a consistent yet functionally diverse decomposer community (Cantoran et al. 2023), whose composition is influenced by initial necromass chemistry (Brabcová et al. 2018; Fernandez and Kennedy 2018; Beidler et al. 2020), which in turn, may impact the chemical fingerprint of SOM (Domeignoz-Horta et al. 2021). Maillard et al. (2023a) found that relative to other edaphic factors (i.e., soil pH, moisture and temperature), soil bacterial richness and fungal community composition were the strongest ecological predictors of fungal necromass decay. In early decomposition, fungal necromass is dominated by saprotrophic fungi (i.e., fast growing moulds and yeasts) and copiotrophic bacteria (Brabcová et al. 2016; Kennedy and Maillard 2023) that can capitalize on an abundance of labile, C-, and N-rich compounds (See et al. 2021). Fast-growing microbial taxa may have lower carbon use efficiency (CUE), meaning they respire more C than they convert into biomass (Manzoni et al. 2018), which may limit the persistence of necromass derived C (Štursová et al. 2012; Adingo et al. 2021). It has also been shown that high concentrations of the cell wall pigment melanin have been shown to slow the uptake of fungal necromass C and N by both bacterial and fungal communities during decomposition (Maillard et al. 2023b). Melanins are high molecular weight, hydrophobic polyphenols that often complex with proteins, and carbohydrates (Bell and Wheeler 1986; Butler and Day 1998; Rillig et al. 2007), potentially limiting C and N release from fungal necromass. Additionally, melanized hyphae may bind more readily to soil minerals or have a higher sorption affinity than hyphae without melanin (Fomina and Gadd 2003). Because melanized hyphae can comprise greater than 50% of total hyphal mass in some forests (Hunt and Fogel 1983; Van der Wal et al. 2009; Clemmensen et al. 2013; Siletti et al. 2017), melanization may be a key factor in predicting the formation of soil mineral-associated fungal C and N.

The molecular composition of fungal cells reflects the varied ecology of individual fungal species and results in a complex mixture of detrital proteins, polysaccharides, and phenols post-senescence (See et al. 2021). The two-pool nature of fungal necromass decay supports the existence of a larger labile or ‘fast’ decaying fraction (~80% of initial mass) and a smaller recalcitrant or ‘slow’ decaying fraction (~20% of initial mass; Fernandez et al. 2019; Ryan et al. 2020; See et al. 2021). Labile substrates form dissolved organic matter (DOM) that can be assimilated by microbes and converted into residues and biomass (i.e., the microbial synthesis pathway of SOM formation), which may then become “entombed” via organo-

mineral interactions (Cotrufo et al. 2015; Liang et al. 2017). Alternatively, DOM may bind directly to soil minerals (i.e., the direct sorption pathway of SOM formation; Kalbitz et al. 2005; Cotrufo et al. 2015), with the strength of mineral-bonding being higher for polar compounds (e.g., carboxyl and phenolic acids) compared with compounds that bind through weaker hydrogen bonds or van der Waals forces (e.g., simple sugars; Jagadamma et al. 2012; Sokol et al. 2019). In general, peptidic compounds have a strong affinity for a wide array of mineral and organic surfaces in soils and make up the largest store of soil organic N (Theng 2024; Rillig et al. 2007; Norén et al. 2008). Currently, it is unclear how different necromass chemical properties might promote fungal C and N persistence in soil together or independently, as few studies have tracked the stabilization of both fungal necromass C and N simultaneously (but see Schweigert et al. 2015; Buckeridge et al. 2022; Wang et al. 2024). Moreover, additional studies are needed to interrogate the links between necromass chemistry and different SOM formation pathways under a range of diverse soil properties.

To gain insights into how the intrinsic chemical properties of fungal necromass interact with both soil microbial and mineral properties to determine fungal C and N persistence, we performed two experiments utilizing necromass of high and low melanin phenotypes of the same fungal species, *Hyaloscypha bicolor*. In the first experiment, we decayed dual enriched (^{13}C and ^{15}N) low and high melanin necromass in either live or sterilized soils differing in initial microbial and physicochemical properties. Specifically, we utilized six temperate forest soils representing a gradient of increasing iron-oxide (FeOx) content collected from various sites in Indiana, USA. We predicted that increased FeOx and clay content would promote the retention of fungal-derived C and N in mineral associated organic matter (MAOM). Beyond soil mineral properties, we were interested in the potential for initial microbial community structure to predict the transformation of fungal necromass into MAOM. We hypothesized that initial microbial properties, specifically related to decomposer guild composition and relative abundance (e.g., fungal saprotrophs and bacterial copiotrophs), would influence necromass-derived MAOM formation and chemistry, but likely to a lesser extent than soil mineral properties. We predicted that MAOM formation would be higher in sterile compared to live soils due to direct adsorption of soluble necromass compounds in the absence of microbial decomposers. Further, we hypothesized that the chemical classes available for adsorption onto iron oxide minerals would differ between necromass types. To test this hypothesis, we performed a second experiment to identify compounds from low and high melanin that adsorbed directly onto synthesized goethite, an iron oxide mineral ubiquitous in soils, using simultaneous infrared and potentiometric titration (SIPT). Collectively, these two experiments allowed us to assess the relative amounts of fungal necromass-derived C and N as well as the necromass chemical constituents that persist as MAOM. Given efforts to increase soil C globally (Minasny et al. 2017), we require a more

mechanistic understanding of how microbial necromass is converted into MAOM and the factors that predict its persistence.

Methods

Fungal Necromass Preparation

Necromass Generation

We generated dual ^{13}C and ^{15}N enriched fungal necromass ex-situ from *Hyaloscypha bicolor* (previously *Meliniomyces bicolor)*, an ascomycete fungus known to form ectomycorrhizal and ericoid mycorrhizal associations with temperate plant species (Grelet et al. 2009; Fehrer et al. 2019). Depending on culture oxygenation, *H. bicolor* will produce both high and low melanin phenotypes and therefore has been utilized in a number of different previous studies to test the effect of melanization on necromass decay independent of species differences (Fernandez and Kennedy 2018; Ryan et al. 2020; Maillard et al. 2023b). Mycelial plugs (3mm diameter) taken from modified Melin-Norkans (MMN) agar plates were transferred into either 125- or 250-ml Erlenmeyer flasks containing 100 ml of liquid MMN media (pH = 5). Different sized Erlenmeyer flasks were used to vary liquid levels without changing media volume, as it has been demonstrated that increasing the submersion level of *H. bicolor* reduces cell wall melanization without altering fungal mass or growth rates (Fernandez and Kennedy 2018). The sole carbon source in the media was D-Glucose-$^{13}C_6$, (99 atom % ^{13}C; Cambridge Isotope Laboratories) together with D-Glucose-$^{12}C_6$, for a targeted enrichment of ~1 atom % or ~37 ‰ (see Table S1 for initial necromass isotopic enrichment values). As an N source, we added Ammonium-^{15}N (99 atom % ^{15}N; Cambridge Isotope Laboratories) in combination with ^{14}N chloride for a targeted enrichment of ~2 atom % or ~700 ‰. Enrichment was higher for N because of its disproportionally smaller mass relative to the C contained in necromass (Table S1) and enrichment targets were set according to the highest isotopic standards available through the Purdue Stable Isotope (PSI) Facility, West Lafayette, IN, USA.

Flasks were shaken at 80 rpm in the dark for 30 days or until colonies stopped growing. During harvest, fungal biomass was rinsed with distilled water (di-H_2O) over 0.5 mm polyester mesh and any remaining agar from the mycelial plugs was carefully removed with forceps. The rinsed biomass was then dried at 25°C for 48 hours, which was shown to be sufficient for killing the fungus, while limiting chemical transformation. To homogenize the resulting necromass, dried fungal biomass was lightly ground using a mortar and pestle and passed through a sieve stack; the cumulative mass retained on the 2 mm and 0.125

mm sieves was considered fungal necromass. Fungal necromass was subsampled for initial chemistry measurements and stored in a desiccator until the start of the incubation.

Initial Necromass Chemistry

Necromass subsamples were ground to a fine powder using a GenoGrinder (SPEX® SamplePrep; 1600 rpm for 1 minute) and analyzed for total C and N, as well as $\delta^{13}C$ and $\delta\ ^{15}N$ using an elemental analyzer coupled to a gas-isotope ratio mass spectrometer (PDZ Europa Elemental Analyzer coupled to a Sercon 20-22 IRMS) at the PSI facility. To approximate the proportion of initial C quality fractions (e.g., cell soluble versus acid unhydrolyzable fractions) we used forage fiber analysis procedures as described by ANKOM Technology and used in previous fungal necromass studies (See et al. 2021; Maillard et al. 2023b). To determine the mass of the cell soluble fraction, which includes simple carbohydrates, lipids, and soluble proteins, we quantified the portion of necromass lost after constant agitation in a neutral detergent solution at 100°C for two hours. To determine the mass of the acid unhydrolyzable fraction, which consists of aromatic compounds including melanin, residual necromass was then extracted with a strong acid (72% H_2SO_4) at room temperature for three hours with repeated agitation (every 30 minutes; Maillard et al. 2023b).

Soil Microcosm Preparation

Soil sampling

Soils were taken from hardwood forest plots at sites established by the Indiana Department of Natural Resources (IDNR) as part of the Continuous Forest Inventory (CFI) program (See Fig. 1 for sampling locations and soil series information). We selected soils from six CFI plot sites (diameter = 14.6 m) sampled in the summer of 2020 (Late May-Late July). Soil samples were collected at 90° and 270° azimuth, 7.62m from the center of the plot at a depth of 10-20cm (diameter = 5cm). Soil cores from a given site were homogenized over a 2 mm sieve and air dried. For specific site soil series and overstory information see Table S2.

Initial soil physicochemical measurements

To measure soil pH, a subsample of air-dried soil (5 g) was shaken at 180 rpm in 40 mL of 0.01M $CaCl_2$ for 30 minutes and vortexed prior to taking readings with a benchtop SymPHony Benchtop pH Meter (VWR International, Radnor, PA, USA). The percentage of clay within soils was measured using a standard hydrometer procedure (Gavlak et al. 2005; see KBS LTER protocol for specifics). To estimate concentrations of noncrystalline and poorly crystalline Fe-oxides (FeOx) in initial soils, we measured

oxalate-extractable Fe content (Ross and Wang 1993; Craig et al. 2022). In short, 40 mL of 0.2 M $(NH_4)_2C_2O_4$ (pH = 3) was added to 0.2 g (dwt equivalent) of soil. After shaking in the dark for four hours, samples were gravity filtered (Whatman No. 40 filter paper) and extracts were refrigerated until analysis (within 4 days). Iron in the extract was determined using atomic-adsorption spectrometry; Fe was atomized using an Aanalyst 800 air-acetylene flame (Perkin Elmer, Waltham, MA, USA).

Initial soil microbial community measurements

To identify fungal and bacterial communities in initial soils (n = 3 samples per site; 18 samples total), we applied a two-step high throughput sequencing (HTS) DNA metabarcoding approach. Briefly, total genomic DNA was extracted from soils using a Qiagen DNEasy PowerSoil Kit (Qiagen, Benelux BV) according to the manufacturer's instructions. Extracted DNA from each sample was first PCR amplified targeting the ITS2 region of the fungal rRNA operon (5.8S-Fun and ITS4-Fun primer pair; Taylor et al. 2016) and the V4 region of the bacterial 16S rRNA gene (515F-806R primer pair; Caporaso et al. 2012), respectively. In a shorter second PCR, unique Golay barcodes and sequencing adaptors were added to samples with amplicons. Further details on PCR reagents and conditions are available in Maillard et al. (2023b). Amplified products were quantified using a Qubit dsDNA HS Fluorometer (Life Technologies, Carlsbad, CA, USA) and cleaned using a Charm Just-a-Plate Purification and Normalization Kit (Charm Biotech, San Diego, CA, USA). We included negative controls, consisting of a lysis tube without soil during DNA extraction and PCR blanks (molecular grade water used in place of DNA template), as well as positive controls consisting of fungal synmock (Palmer et al. 2018) or bacterial zymock (Zymo Research, Irvine, CA,USA) communities. Each of the samples were pooled into a single library and sequenced at the University of Minnesota Genomics Center using the 2 x 300 base pair (bp) paired-end MiSeq Illumina platform.

Fungal Necromass Incubation

Live soil conditions

Incubations were carried out in 50 ml centrifuge tubes (Chang Bioscience, Inc., Fremont, CA, USA) with modified caps, which included a 0.2 µm vent filter to allow for air exchange and central needle (14 gauge 1 ½'' needle) for sterile water additions (needle was capped when not in use; See Fig. S1A-B). We added 5 g (dwt equivalent) of soil to each microcosm and one week prior to the start of the incubation soils were brought up to 65% water holding capacity (WHC). Three soil microcosms were prepared for each soil-necromass combination & soil only controls (54 microcosms total). To begin the incubation, 70 mg of necromass was added to microcosms and soils were mixed using a dissecting needle. To maintain

consistency among treatments we mixed soil only controls in a similar manner as microcosms receiving necromass additions. Throughout the duration of the 38-day incubation microcosms were kept in the dark at 20 ◦C and soils were held at 65% WHC via weekly additions of sterile di-H_2O in a laminar flow hood. To stop incubations, soils were dried at 60°C for 4 days.

Sterile soil conditions

For a subset of the sites (C153, C169, and C61), we autoclaved dry soils and necromass separately (60-minute gravimetric cycle) to mimic abiotic conditions in more complex soils (see Table S1 for initial necromass isotopic values). In short, we brought sterile soils up to 65% WHC one week prior to the start of the incubation by adding sterile water under aseptic conditions and mixed in 70 mg of autoclaved necromass using a flame sterilized dissecting probe. There was not enough initial autoclaved necromass remaining to measure initial C quality fractions. Three soil microcosms were prepared for each soil-necromass combination as well as three soil only controls (27 microcosms total). Sterile soil microcosms were maintained and sampled in a similar manner as live soil microcosms.

Necromass ^{13}C & ^{15}N Tracing

Necromass-derived MAOM measurements

We isolated mineral-associated organic matter (MAOM) using a modified size fractionation procedure (Cambardella and Elliott 1992; Craig et al. 2022). To float off undecomposed necromass that might leach DOM to mineral associated soil pools during fractionation, we added 30 mL of di-H_2O inverted five times and centrifuged at 2500 rpm for 10 minutes. Necromass was carefully removed with forceps and dried for 48 h at 60°C. The clear supernatant was discarded to remove DOM. The soil pellet was resuspended in 5% (w/v) sodium hexametaphosphate, shaken (120 rpm) for 24 hours and then washed through a 53-μm sieve. Soil that passed through the sieve (clay + silt sized fraction) was considered the MAOM fraction, dried and ground for %C, δ^{13}C, %N, and δ^{15}N analysis through the PSI facility.

Isotopic Mixing Models

The fraction of necromass-derived mineral associated organic C and N relative to total MAOM-C and N ($f_{Necro-MAOM}$) was calculated using two-end member mixing models (Comeau et al. 2013; Buckeridge et al. 2022).

$$f_{Necro-MAOM} = \frac{\delta_{MAOM} - \delta_{Control}}{\delta_{Necro} - \delta_{Control}}$$

Where δ_{MAOM} is the measured $\delta^{13}C$ or $\delta^{15}N$ value for the mineral associated organic matter fraction for soils amended with necromass, $\delta_{Control}$ is the average $\delta^{13}C$ or $\delta^{15}N$ value for the MAOM fraction in soil only control samples, and δ_{Necro} is the average initial $\delta^{13}C$ or $\delta^{15}N$ value for each necromass type. The $f_{Necro-MAOM}$ value was multiplied by the mass of the C or N in the MAOM fraction at the end of the 30 day incubation to calculate the amount of necromass-derived C or N. Data are presented as the amount of necromass derived MAOM-C or -N formed relative to initial necromass C or N (% added necromass C or N).

Diffuse Reflectance Infrared Fourier Transform Spectroscopy

We used DRIFTS to investigate the biochemical composition of mineral associated organic matter (MAOM) generated after the 38-day incubation. Briefly, each MAOM sample was mixed with KBr at a 1% mass/mass ratio and analyzed by DRIFTS on a FTIR spectrometer (Bruker Vertex 80 v, Ettlingen, Germany) in a temperature-controlled room at 21°C. Sixty-four scans were averaged across the 4000–400 cm^{-1} range at a resolution of 4 cm^{-1}. Background subtraction was performed using a pure KBr spectrum, and a baseline correction was applied to eliminate baseline distortions. Both background subtraction and baseline correction were carried out in OPUS software (Bruker, Ettlingen, Germany), and peak heights were normalized by calculating z-scores. Peaks were identified based on the literature on the biochemical composition of soil organic matter (Ellerbrock and Kaiser 2005; Artz et al. 2008; Pärnpuu et al. 2022). Further, multiple annotations have been proposed for some peaks since MAOM is composed of both minerals and organic compounds, and some regions are characteristic of both (Table S3; Stuart 2004). Additionally, low and high melanin necromass samples were analyzed by DRIFTS following the aforementioned procedure.

Simultaneous Infrared and Potentiometric Titration

Goethite synthesis

To assess the capacity for necromass-soluble compounds to adsorb onto soil minerals, we utilized goethite as a model mineral. Naturally occurring in forest soils (Krumina et al. 2017), goethite was synthesized following the method described by Villacís-García et al. (2015). A 2.5 M NaOH solution was slowly added to a 0.5 M $Fe(NO_3)_3 \cdot 9H_2O$ solution under stirring and N2 bubbling until the pH reached approximately 12. The product was aged at 60 °C for 7 days. The suspension was then dialyzed with a dialysis bag (12-14 kDa) in MiliQ water in a cold room at 4 °C, replacing the MiliQ water every 12 hours

until its electrical conductivity was less than 2.0 μS cm^{-1}. The goethite product was transferred to a polyethylene bottle, purged with N_2 gas to remove carbonate species, and stored under 4°C. The concentration of the goethite suspension was determined to be 10.99 g $^{l-1}$. The morphology of goethite particles was assessed for synthesis success by dropping suspensions onto C-coated copper grids, air-drying, and observing with a TEM (JEOL-1400 PLUS) operating at 100 keV. The morphology of synthesized goethite (Fig. S2) is typical for this iron oxide.

Adsorption of necromass compounds on goethite

The adsorption of fungal necromass compounds onto goethite was assessed by infrared spectroscopy using the Simultaneous Infrared and Potentiometric Titration (SIPT) method, as described by Krumina et al. (2017) and Tian et al. (2020). For the adsorption analysis, goethite over-layers were prepared on an attenuated total reflectance (ATR) ZnSe crystal by evaporating 0.7 mL of a goethite suspension. The ATR crystal was then coupled to a titration vessel and placed inside an evacuated FTIR (Bruker Vertex 80 v, Ettlingen, Germany) in a temperature-controlled room at 21 °C. A 0.01 M NaCl solution was added to the titration vessel and gently stirred under N_2 gas to mitigate the effects of atmospheric CO_2. The pH was adjusted to 5.0 and maintained constant with an automated, computer-controlled burette system (Methrom 907 Titrando and Tiamo 2.4 software). After equilibrating the over-layer and medium for approximately 24 hours, a background spectrum of 1024 scans was collected. Subsequently, either low or high melanin bags, consisting of 80 mg of dry necromass in 40 µm polyester mesh bags (Sintab, Malmö, Sweden), were immersed in the vessel under constant stirring. IR collection time was set at 256 scans per spectrum. IR spectra were recorded between 700–4000 cm^{-1} at a resolution of 4 cm^{-1} over one day, with one spectrum recorded every 3.56 minutes, amounting to roughly 400 spectra per necromass type. Retained spectra ranged from 920 to 3050 cm^{-1}. Peaks in the final spectra (number 400) for both necromass types were annotated based on literature on the biochemical composition of fungal biomass and necromass (Dzurendova et al. 2020; Langseter et al. 2021; Maillard et al. 2023c). Necromass remaining in the mesh bags after incubation accounted for 69.7% and 68.3% of the initial mass for low and high melanin necromass types, respectively, suggesting similar leachate sizes.

Data Processing and Statistical Analyses

All statistical analyses were performed in R version 4.3.1 (2023-06-16). Response variables that did not meet assumptions of normality were transformed or analyzed via non-parametric tests indicated below. Means are presented in text and tables plus or minus one standard deviation (SD).

Initial Necromass Data

Analysis of variance (ANOVA) was used to test for differences in initial necromass $\delta^{13}C$ between necromass types (high vs low melanin), sterilization treatment (autoclaved vs. non-autoclaved) and their interaction. Initial necromass % C, % N, and $\delta^{15}N$ did not meet the assumptions of ANOVA (data were non-normal and had unequal variances), as a result, we collapsed necromass type and sterilization treatment into one factor and performed Welch's Analysis of variance ANOVA with Games–Howell post hoc tests. Because sterilization treatment did not have an effect on initial $\delta^{13}C$ or $\delta^{15}N$ (Table S1), autoclaved and non-autoclaved necromass isotopic values were combined and mean values were used for high and low melanin necromass initials.

Microbial Community Data

Bioinformatic processing of HTS data was performed using the amptk pipeline (Palmer et al. 2018, v1.5.4). Briefly, we removed primers and then trimmed sequences to 300 bp. Paired reads were denoised using DADA2 algorithm (Callahan et al. 2016), using the default parameters (minLen = 50, maxN = 0, truncQ = 2, maxEE = 2), and then clustered into OTUs at 97% similarity. To account for index bleed between samples, read counts in the OTU × sample matrices were adjusted using 1% as the filter percentage. To assign taxonomy, we used a hybrid algorithm integrating results from a USEARCH global alignment against the UNITE (v8, Nilsson et al. 2019) and RDP (training set 19, Wang and Cole 2024) databases, including both UTAX and SINTAX classifiers. Data are deposited in the NCBI Short Read Archive (Bioproject # for bacteria PRJNA1094420; for fungi PRJNA1094416).

From the original 18 samples, 2 were removed due to low sequence totals for both bacteria and fungi. To account for differences in sequence reads among the remaining 16 samples, the bacterial and fungal OTU table was rarefied to 43280 and 249696 reads per sample, respectively. Fungal OTUs were classified by trophic mode using FUNGuild (Nguyen et al. 2016). When there were multiple fungal guilds assigned to a single OTU, the most commonly occurring lifestyle were determined using the FungalTraits database (Põlme et al. 2020). We assigned bacterial OTUs to copiotrophic and oligotrophic trophic modes based on Trivedi et al. (2017). Briefly, bacterial OTUs belonging to the phylum Bacteroidetes and classes alpha-Proteobacteria, beta-Proteobacteria and gamma-Proteobacteria were defined as copiotrophs, whereas OTUs belonging to phylum Acidobacteria and class delta-Proteobacteria were defined as oligotrophs. ANOVA with type III errors ('Anova' function in the Car package) was used to test for site differences in mean richness (number of unique OTUs) and diversity (Shannon diversity) in bacterial and fungal community. Bacterial copiotroph richness as well as oligotroph relative abundance and richness were log transformed to meet the assumption of normality. We investigated differences in bacterial and fungal

community composition across sites by calculating a Bray-Curtis dissimilarity matrix with read-abundance data using the 'metaMDS()' function in the Vegan package (Oksanen et al. 2022). To visualize the soil physiochemical variables covarying with microbial community structure across sites, we fit vectors to non-metric multidimensional scaling (NMDS) ordination plots using the 'envfit' function in the Vegan package. Permutational multivariate analyses of variance (PERMANOVA) was applied to assess site effects on microbial community composition.

MAOM Formation and DRIFTS Data

ANOVAs were used to test for significant effects of necromass type and site, as well as their interaction on MAOM formation (MAOM-C and N data were log transformed prior to analysis for sterile microcosm soils). Post-hoc tests were carried out using Sidak multiple comparison in the Emmeans package (Lenth 2022). Correlations between initial soil properties and response variables were determined by calculating Pearson's correlation coefficients. Significant correlations were further analyzed in either bilinear or mixed effect multiple linear regression models. Mixed effect models were used to examine the combined effects of soil mineral and microbial properties on MAOM formation, using site as a random effect (1| site). To eliminate unit dimension effects, all independent variables were standardized (average = 0 and SD = 1). A variance inflation factor of three or less was used to eliminate multicollinear variables. The optimal model was selected using Akaike information criterion (AIC) by identifying the lowest AIC and highest R^2 values after removing variables with a VIF > 3. Principal component analysis (PCA) biplots of DRIFT spectra were used to visualize separation of MAOM samples based on site or necromass treatment. Principle component loadings were plotted against wavenumber to identify peaks that correspond with the first two PCA axes.

SIPT Spectral Data

IR peak heights were identified using the quick peaks function with a constant baseline in OriginLab (Northampton, MA, USA). We included peaks that fell within a range of ± 10cm^{-1} of annotated peaks (Table S3). To explore changes in peak height over time, we fit asymptotic regression models for annotated peaks, for both high and low melanin necromass-goethite suspensions using the 'nls' and 'SSasymp' functions in the Stats package. The model below describes peak height (y) as a function of hourly time (x), where $\emptyset_1$ is the horizontal asymptote on the right of the curve or the maximum value of y, $\emptyset_2$ is a numeric parameter representing the response when the input is zero and $\emptyset_3$ is the natural logarithm of the rate constant (lrc; Drever et al. 2023).

$$y = \emptyset_1 + (\emptyset_2 - \emptyset_1)exp[-exp(\emptyset_3)x]$$

Results

Initial physicochemical and microbial properties of microcosm soils

While the sites were primarily selected to vary in soil oxalate-extractable Fe (Fig. 1A), FeOx concentration was significantly correlated with clay content ($r = 0.95$, $p < 0.01$) and total C ($r = 0.94$, $p < 0.01$). Across sites, initial microbial community composition varied more than diversity (Table S4), with PERMANOVA results demonstrating significant differences in the soil fungal ($R^2 = 0.95$, $F = 35.9$, $p = 0.01$) and bacterial ($R^2 = 0.90$, $F = 17.2$, $p = 0.01$) communities by site (Fig. 2B-C). Sites with increased relative abundances of fungal saprotrophs also had higher relative abundances of bacterial copiotrophs ($r = 0.64$, $p = 0.01$), while bacterial oligotroph relative abundance and bacterial OTU richness increased with increasing soil pH, FeOx, clay and C content (Fig. S3).

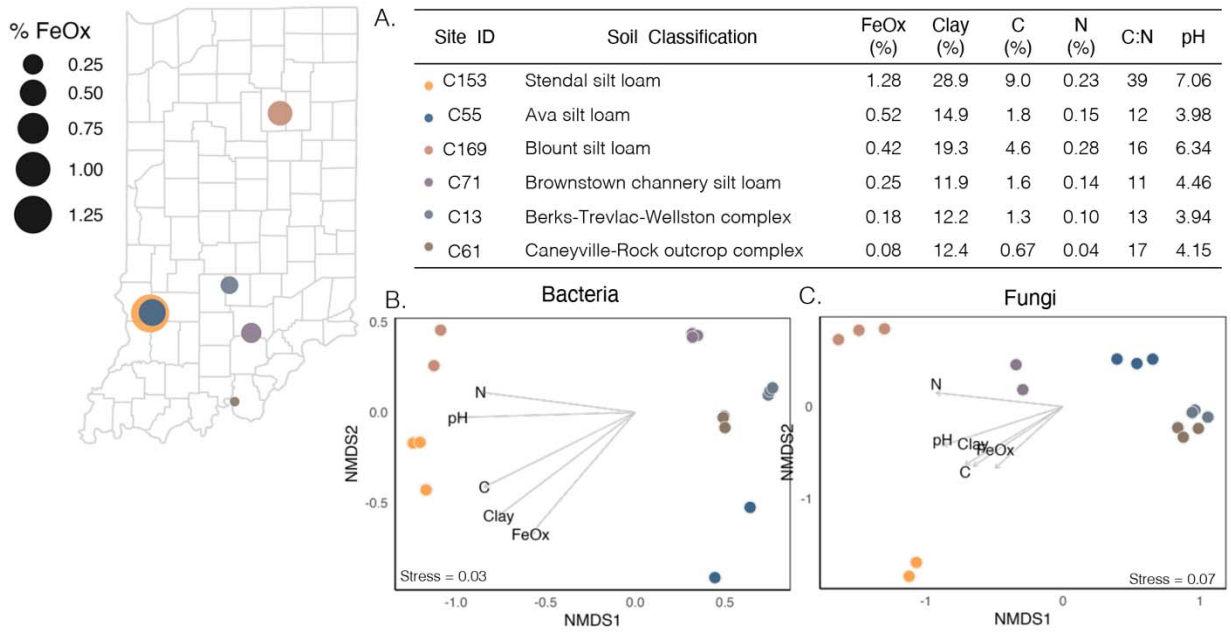

Site ID	Soil Classification	FeOx (%)	Clay (%)	C (%)	N (%)	C:N	pH
C153	Stendal silt loam	1.28	28.9	9.0	0.23	39	7.06
C55	Ava silt loam	0.52	14.9	1.8	0.15	12	3.98
C169	Blount silt loam	0.42	19.3	4.6	0.28	16	6.34
C71	Brownstown channery silt loam	0.25	11.9	1.6	0.14	11	4.46
C13	Berks-Trevlac-Wellston complex	0.18	12.2	1.3	0.10	13	3.94
C61	Caneyville-Rock outcrop complex	0.08	12.4	0.67	0.04	17	4.15

Figure 1. A. Site locations and initial physicochemical properties of six different soil types chosen to represent contrasting soil iron oxide (FeOx), clay, carbon (C), and nitrogen (N) content, C to N ratio and pH. NMDS ordinations for B. Bacterial and C. Fungal communities with soil property vectors.

Fungal necromass derived C and N stabilization in live microcosm soils

After 38 days of incubation, we found that 7 times more initial fungal necromass N (41.6 ± 6.3%, CV = 0.15) was incorporated into MAOM relative to necromass C (5.74 ± 1.1%, CV = 0.19). Site identity explained 52% and 35% of the variation in necromass-derived MAOM-C ($F = 8.39$, $p < 0.001$) and MAOM-N ($F = 3.04$, $p = 0.03$) formation, respectively. The accumulation of fungal derived MAOM-C

ranged from 4.41 ± 0.88% of initial necromass C for soils from the Jackson County site (C71) to 6.92 ± 1.1% of initial necromass C for soils from the Sullivan County site (C153) which also had the highest initial clay and FeOx content. Fungal derived MAOM-N also differed among sites (Fig. S4), ranging from 37 ± 10% for soils from the Jackson County site (C71) to 48 ± 6% of initial necromass N for soils from Greene County site (C55). Though the greatest differences in MAOM formation were among sites, necromass type significantly affected MAOM-C formation (Fig. 3A, $F = 8.09$, $p < 0.01$) and had a moderately significant effect on MAOM-N formation (Fig. 3B, $F = 3.85$, $p = 0.06$) (Fig 3B; Table S5). On average, low melanin necromass contributed 11% more to MAOM-C (HM: 5.4 ± 1.0%, LM: 6.1 ± 1.0%) and 9% more to MAOM-N (HM: 39 ± 7%, LM: 43 ± 5%) than high melanin necromass and differences were consistent across sites (Table S5 & Fig. S4). MAOM-C and N formation were coupled ($R^2 = 0.42$, $p = 0.02$), but only for soils amended with high melanin necromass. However, this trend was largely driven by a single point (Fig. S5).

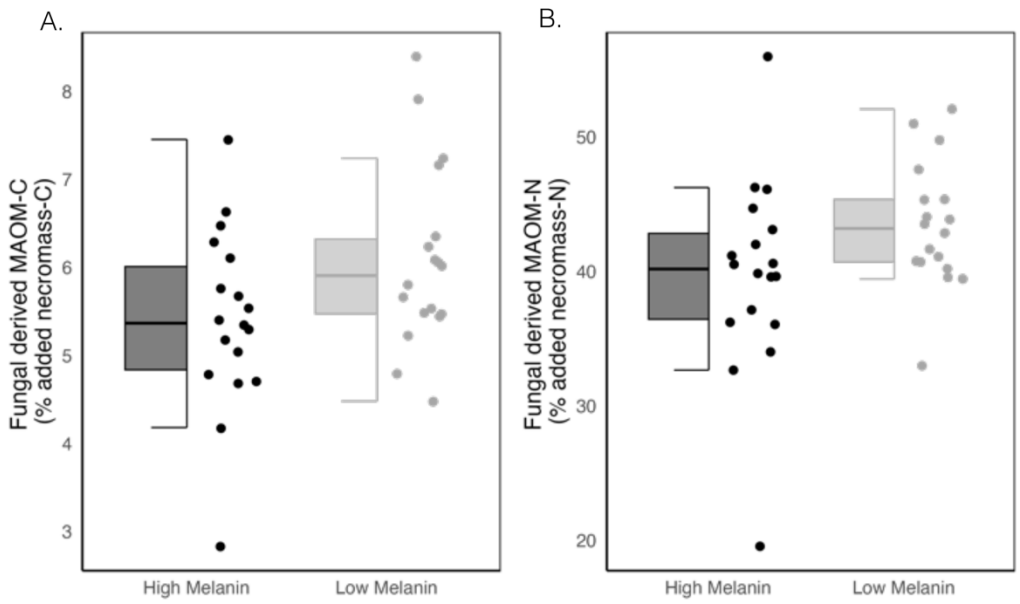

Figure 2. Box and whisker plots of fungal necromass derived mineral associated organic matter (MAOM) A. carbon (C) and B. nitrogen (N) formation in live soil microcosms after a 38-day incubation.

Correlations between initial soil predictors and MAOM formation differed between necromass types (Fig. S3). For soils amended with high melanin necromass, necromass-derived MAOM-C was negatively correlated with initial fungal saprotroph abundance ($r = 0.60$, $p = 0.03$). For soils amended with low melanin necromass, MAOM-C formation was positively correlated with soil FeOx ($r = 0.74$, $p < 0.01$), clay content ($r = 0.71$, $p < 0.01$), and total C ($r = 0.63$, $p = 0.02$), as well as initial oligotrophic bacterial abundance ($r = 0.73$, $p < 0.01$) and richness ($r = 0.69$, $p < 0.01$; Fig. S3). For both high and low melanin

necromass, fungal derived MAOM-N formation was negatively correlated with bacterial copiotroph relative abundance (Fig. S3).

Table 1: Multivariate linear regression models for fungal necromass-derived mineral associated organic matter (MAOM) carbon (C) and nitrogen (N) formation.

Necromass Type	Response	Predictor	Df	β	β SE	t	p
High Melanin	MAOM-C $R^2 = 0.37$	Fungal Saprotroph Relative Abundance	14	-4.01	1.45	-2.77	0.02
	MAOM-N $R^2 = 0.38$	Bacterial Copiotroph Relative Abundance	14	-3.35	1.20	-2.80	0.01
Low Melanin	MAOM-C $R^2 = 0.77$	Bacterial Composition (NMDS1)	9	-0.77	0.20	-3.93	0.003
		Bacterial Composition (NMDS2)	11	-1.50	0.35	-4.28	0.001
	MAOM-N $R^2 = 0.40$	Bacterial Copiotroph Relative Abundance	9	-3.04	1.18	-2.3	0.03

When examining the combined effects of soil physicochemical and microbial properties on MAOM formation using site as a random effect, microbial predictors were stronger predictors of both MAOM-C and MAOM-N formation (Table 1) but were highly collinear with soil physiochemical properties. The initial relative abundances of fungal saprotrophs alone explained 37% of the variation in high melanin necromass-derived MAOM-C formation. Bacterial community composition (as captured by NMDS axes 1 and 2) explained 77% of the variation in low melanin necromass-derived MAOM-C formation (Table 2). Notably, soils with lower scores along the first and second bacterial NMDS axes formed more necromass-derived MAOM-C and were from sites (C153 & C169) with the highest initial soil pH, % clay, % C, % N and also had the greatest relative abundances of oligotrophic bacteria and lower relative abundances of saprotrophic fungi (Fig. S3). For necromass-derived MAOM-N, initial bacterial copiotroph relative abundance explained ~38% and 40% of the variation from high and low melanin necromass types, respectively, with increased relative abundances of bacterial copiotrophs resulting in less fungal derived MAOM-N accumulation (Table 1).

MAOM chemistry in live soil microcosms

The chemical composition of MAOM from soils at the end of the 38-day incubation was characterized by strong mineralogy associated bands at 3695 – 3621 cm^{-1} assigned to O-H bonds, indicative of either clay or aluminum minerals, as well as Si-O bonds in the 695-474 cm^{-1} region, associated with silicate minerals (Fig. 3A & Table S3). The mean intensity of bands at 1284 cm^{-1} and from 940-779 cm^{-1} varied notably among sites, attributed to phenolic and aromatic compounds with C-O and C-H functionalities. While first two principal components explained ~70% of the variation in MAOM chemistry, the PCA plot did

not show strong separation of spectra among necromass amended and soil only controls (Fig. 3B). Instead, the clearest separation occurred between soils originating from the Sullivan County site (C153) and other samples along the first principal component axis (PC1). PERMANOVA results supported the PCA visualization, with site explaining a much more significant amount of spectral variation (R^2 = 0.60, F = 14.4, $p < 0.001$) than necromass type (R^2 = 0.02, F = 1.41, p = 0.20). The loading of PC1was negatively correlated with peaks at 3621-3695 cm^{-1}, 1186-1360, 779-940 cm^{-1}, which together are indicative of oxygenated functionalities associated with clay and silicate minerals (Fig. 3C). These findings support the unique mineralogy of the Sullivan County site (C153), which formed the greatest amount of necromass-derived MAOM-C (Table S6).

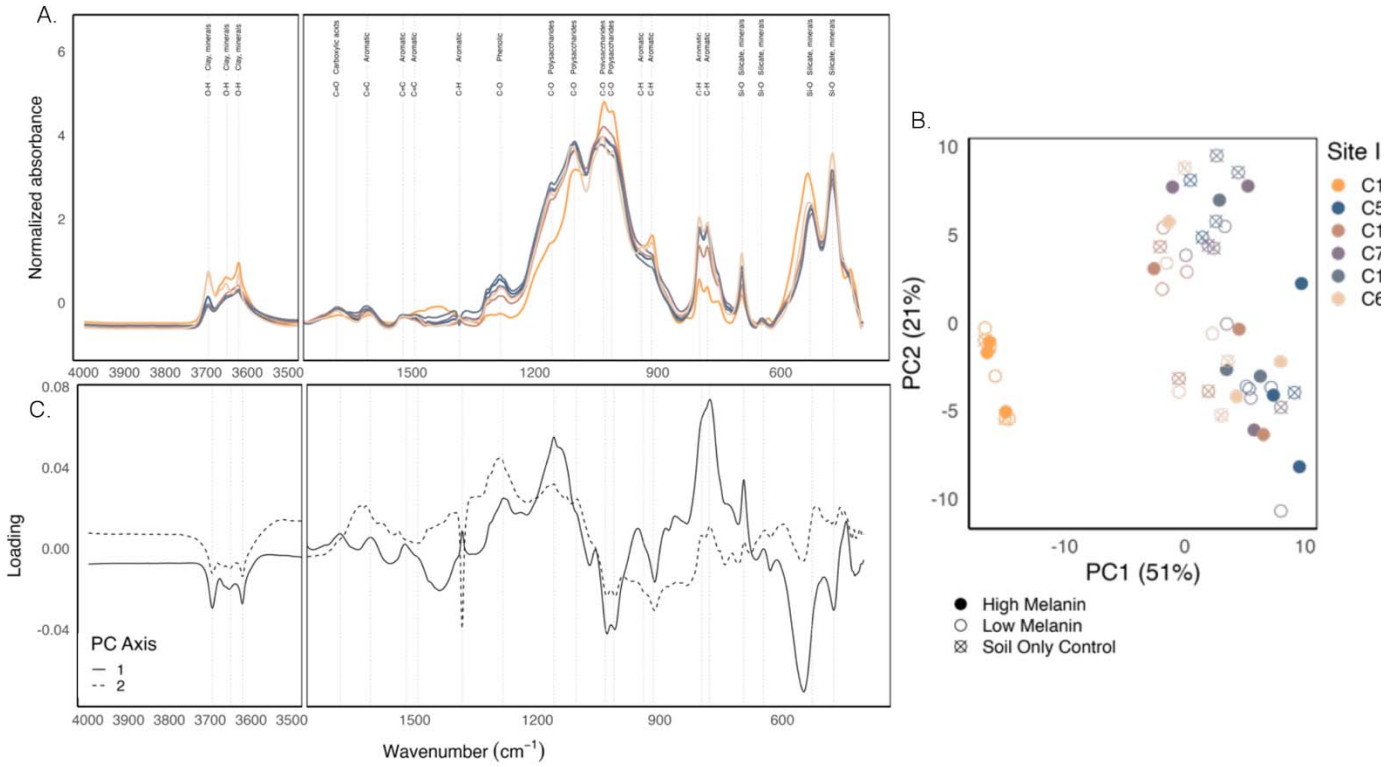

Figure 3. A. Diffuse Reflectance Infrared Fourier transform spectroscopy (DRIFTS) spectra with annotated peaks for mineral associated organic matter (MAOM) grouped by site. B. Principal Component Analysis (PCA) biplot of DRIFT spectra for MAOM from live soil microcosms. C. PCA loadings for the first two principal component (PC) axes.

Fungal necromass derived MAOM formation & chemistry in sterile microcosm soils

More necromass-derived MAOM-C (Fig. 4A) and less MAOM-N (Fig. 4B) accumulated in sterile soils for both high and low melanin necromass types than in live soils (Table S7). Specifically, MAOM-C formation was higher in sterile soils by 50% and 40% for high and low melanin necromass respectively,

while MAOM-N formation was 30% lower from both high and low melanin necromass amendments. Moreover, for soils amended with low melanin necromass, fungal derived MAOM-C was higher in sterile soils despite the autoclaved necromass having lower initial % C (Tables S1 & S8). For the subset of soils (sites C153, C169, C61) with both live and sterile soil microcosms, we did not detect differences in MAOM formation between high and low necromass types regardless of sterilization treatment (Tables S7-8). Similar to live soil microcosms, DRIFT spectra of MAOM from sterile microcosms did not differ between necromass amended and soil only controls (PERMANOVA: $R^2 = 0.01$, $F = 0.59$, $p = 0.70$; Fig S6B). Additionally, spectra did not differ between sterile and live soil only control microcosms (PERMANOVA: $R^2 = 0.01$, $F = 0.14$, $p = 0.9$, Fig. S6C).

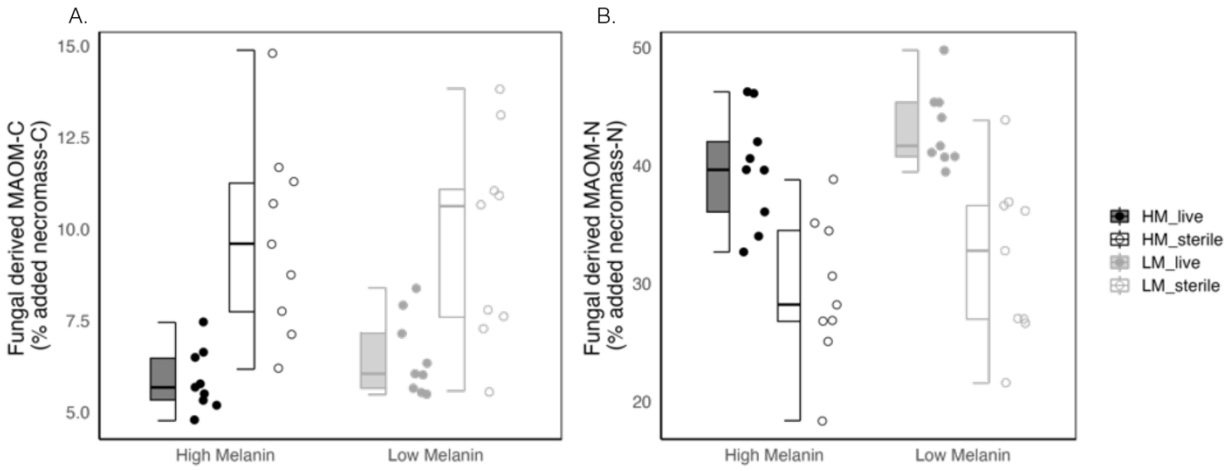

Figure 4: Box and whisker plots of fungal necromass derived mineral associated organic matter (MAOM) A. carbon and B. nitrogen formation in live and sterile (autoclaved soils) after a 38-day incubation. Dark gray boxes and points represent high melanin (HM) necromass and light gray boxes and points represent low melanin (LM) necromass in either live (filled boxes and points) or sterile (open boxes and points) soil conditions.

The adsorption of fungal necromass compounds onto synthesized goethite

With the exception of higher $\delta\ ^{13}C$ enrichment for low melanin necromass, the initial C values did not differ between the two necromass types (Table S1). The cell soluble and unhydrolyzable fractions were also largely equivalent between high and low melanin necromass. Despite these similarities in initial substrate C chemistry, we observed a number of clear spectral differences in the labile compounds that adsorbed onto goethite minerals between necromass types (Fig 6 & Fig S7). Specifically, IR spectra showed much higher intensity of amide bond peaks (N-H & C=O bonds between 1650 cm^{-1} and 1540 cm^{-}

^{1}) for low melanin necromass as well as greater intensity of the 1108 cm^{-1} aromatic bond peak (Fig. 6A). Conversely, IR spectra for high melanin necromass had higher intensities of aliphatic (C-H) and polysaccharide (C-O) bond peaks located at absorbances of 2925 and 1108 cm^{-1}, respectively (Fig 6B). The IR signal intensities also varied over time, with peak heights changing rapidly at first and then stabilizing or reaching an asymptote within 24 hours (Fig. 6B). We found that compounds from high melanin necromass tended to converge to their asymptote (maximum peak height) at faster rates, especially for the aforementioned aliphatic (2925 cm^{-1}) and polysaccharide (1108 cm^{-1}) associated bonds (Fig S7A-C).

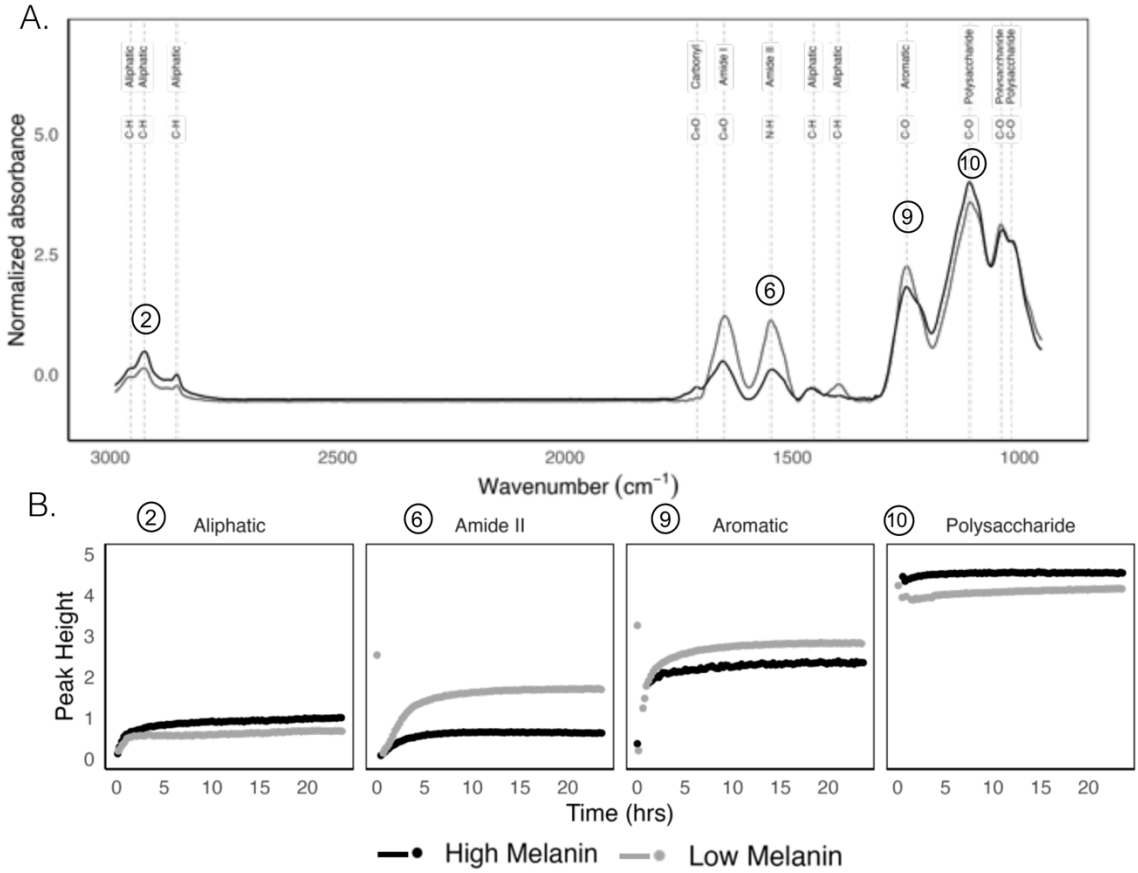

Figure 5: A. Simultaneous infrared and potentiometric titration (SIPT) infrared spectrum (spectra number 400) for high and low melanin necromass suspensions after 24 hours. B. Changes in peak intensity over time for aliphatic (C-H), amide (N-H), aromatic (C-O) and polysaccharide (C-O) derived functionalities (numbers represent peak IDs- see Fig. S7A) from SIPT spectra of high (black line) and low (gray line) necromass compounds adsorbed onto synthesized goethite minerals under abiotic conditions.

Discussion

Long-term soil C and N persistence is thought to be largely determined by associations with soil minerals, with a diversity of microbial inputs and minerals offering numerous means for binding OM (Cotrufo et al. 2013; Kallenbach et al. 2016; Liang et al. 2017; Sokol and Bradford 2019; Lehmann et al. 2020). Here we assessed how initial fungal necromass chemistry interacts with different soil physicochemical and microbial properties to determine fungal necromass C and N stabilization via mineral associations. We hypothesized that MAOM formation and chemistry would differ from high and low melanin fungal necromass inputs, but that soil iron oxide (FeOx) content would be a strong overall predictor of necromass-derived MAOM-C and MAOM-N accumulation regardless of melanization. Though we found spectral differences in the soluble necromass compounds from high and low melanin necromass that adsorbed onto synthesized FeOx minerals, total MAOM-C and MAOM-N formation was similar between necromass types in sterile soils (Figs. 5-6). This suggests that initial substrate chemistry does not directly predict MAOM-C and MAOM-N accumulation across diverse soil mineralogies. Instead, it appears that microbial degradation of fungal necromass, which differs between necromass types, more strongly impacts MAOM-C and MAOM-N formation. This was evident in the live soil microcosms, where bacterial oligotroph relative abundance and initial FeOx content were positively related to MAOM-C formation, but only for soils amended with low melanin necromass. Further, we found that initial microbial community properties were better integrators of physiochemical differences among soils, with relative abundances of different decomposer functional guilds explaining significant variation in MAOM formation across soil types. In particular, we found that initial relative abundances of soil fungal saprotrophs predicted MAOM-C formation from high melanin necromass and initial relative abundances of bacterial copiotrophs predicted MAOM-N formation from both high and low melanin necromass (Table 1). Taken together, these findings point to the potential for different stabilization pathways for C- and N-containing fungal necromass compounds mediated by necromass type, soil properties, and microbial communities, as discussed below.

Necromass derived MAOM-C and N stabilization may be driven by different processes

The persistence of microbial necromass in soil may be promoted abiotically by associating directly with mineral surfaces (direct sorption pathway) or biotically via microbial assimilation (microbial synthesis pathway); in reality, both pathways occur simultaneously and their relative importance for fungal necromass C and N stabilization is unclear (Buckeridge et al. 2020). On average, we show that 8% of total MAOM-C and 20% of MAOM-N originated from fungal necromass decay over a 38-day period. Greater retention of necromass-derived N than C may be due to differences in bond affinities for N-containing compounds and/or greater immobilization of fungal-derived N in living microbial biomass (Omoike and Chorover 2006; Kleber et al. 2007; Wang et al. 2024), which may also decouple MAOM-C

and MAOM-N formation. Nitrogenous compounds bind readily to mineral surfaces (Kleber et al. 2015) and microbes may use them with high efficiency, resulting in N-rich microbial products that then subsequently bind to soil minerals (Cotrufo et al. 2013; Kallenbach et al. 2016). We found that the intensity of N-H bonds from necromass-derived amide compounds increased on goethite minerals within 24 hours, in support of the direct sorption pathway. However, 30% less initial necromass-N was converted into MAOM-N in sterile soils, indicating that microbial synthesis may be the more important pathway for necromass derived MAOM-N formation (Weider et al. 2014; Wang et al. 2020). These findings agree with those of Keiluweit et al. (2012), who tracked ^{13}C and ^{15}N isotopically fungal cell wall residues onto FeOx surfaces during a three-week incubation experiment. That study revealed that amide-N from fungal chitin was consumed by hyphal-associated bacteria, assimilated into newly synthesized bacterial proteins, and adsorbed onto FeOx surfaces. They also found greater enrichment of fungal derived ^{15}N relative to ^{13}C on FeOx minerals, which may be explained by greater microbial assimilation of fungal-N and greater mineralization of fungal-C (Keiluweit et al. 2012; Wang et al. 2024).

Our SIPT analyses also showed evidence for direct sorption of C-containing bonds from carboxylic acids, a functionality known to be important in stabilizing microbial necromass via interactions with FeOx minerals (Lützow et al. 2006; Kleber et al. 2015). We also found that less necromass C became MAOM-C in live soils, suggesting that microbial synthesis did not promote the retention of necromass C to the same extent as necromass N. Buckeridge *et al.* (2020) also found higher retention of fungal necromass ^{13}C in sterile compared to live soils in a short-term (3 day) study in grassland soil microcosms. Given the fast-decaying nature of fungal necromass (Fernandez et al. 2016; Brabcová et al. 2016), it is possible that the majority of necromass C was lost via respiration (Buckeridge et al. 2020). We did not, however, track necromass-derived $^{13}CO_2$ loss or incorporation into other soil pools (microbial biomass, dissolved organic matter, or particulate organic matter), making it challenging to differentiate between abiotic and biotic processes in stabilizing fungal necromass-C. Additionally, the steam sterilization of soils may have altered the solubility or leaching of the pre-existing SOM prior to necromass additions (Egli et al. 2006), although we did not find spectral differences in MAOM chemistry after 38 days. Despite these issues, when considered together, our results demonstrate a high potential for the microbial synthesis pathway to dominate fungal necromass-derived MAOM-N formation and for microbial processing to limit fungal necromass-derived MAOM-C formation.

Initial necromass chemistry more strongly influences MAOM formation than MAOM chemistry

Among fungal species, initial substrate chemistry has been shown to be an important control on necromass decay (Fernandez and Koide 2012, 2014), with increased melanin content consistently slowing

necromass decomposition across a range of soil conditions (Fernandez and Kennedy 2018; Fernandez et al. 2019; Maillard et al. 2020; See et al. 2021). Consistent with this, we found that high melanin necromass contributed less C and N to MAOM when compared with low melanin necromass in our live soil microcosms. Melanin has been shown to limit microbial uptake of necromass C and N during both early (7-14 days) and later (35-77 days) stages of decay (Maillard et al. 2023b), likely also preventing microbial assimilation in this study. We suspect that decayed melanized necromass remained in the light soil fraction as particulate organic matter (POM) rather than becoming mineral-bound, although our study design did not allow for the physical fragmentation of necromass by detritivores and likely limited the abundance of microbes with the oxidative enzyme capacity needed to degrade melanin (Fernandez and Kennedy 2018). Additionally, melanin has been shown to form complexes with N-rich cell wall components like chitin, further reducing decomposer access to labile sources of N (Bull 1970; Fernandez and Koide 2014; Ryan et al. 2020). Our SIPT experiment showed much less adsorption of Amide I and Amide II in high melanin necromass, indicating that melanization likely inhibited N association at mineral surfaces, possibly due to the aforementioned protein-melanin complexes in the fungal cell wall. Increased availability of labile N, either for direct sorption or microbial assimilation. Overall, these findings suggest that melanization limits fungal necromass C and N stabilization by inhibiting microbial decomposition (Maillard et al. 2023b).

Although we found differences in MAOM-C formation between necromass types, the chemical analyses of MAOM generated after 38 days did not differ between soils amended with high and low melanin necromass. Our ability to detect differences in MAOM chemistry in necromass amended soils may have been restricted by the short time span of the study and relatively small starting amounts of necromass. Further, we emphasize that it is important to note that MAOM is rich in minerals, which, like organic compounds, absorb infrared light and thus DRIFTs peaks could be indicative of either organic or mineral compounds or a combination of both. Notwithstanding difficulties in differentiating peaks between organic and mineral functionalities, the strongest spectral differences in ordination space were among soils from the Sullivan County site (C153) and the other five sites. In addition to being a poorly drained riparian soil, differences in the dominant tree species at the Sullivan County site may have contributed to spectral variation in MAOM chemistry. Dominant at the Sullivan County site, *Robinia pseudoacacia*, is an early successional N-fixer that has been shown to increase soil N availability and litter quality (high N,low lignin leaf litter) in pine-oak forests (Rice et al. 2004), which may have contributed to the soil's unique SOM chemistry. Though microbes produce chemically diverse MAOM (Golchin et al. 1996; Kallenbach et al. 2016), the direct incorporation of plant compounds into MAOM (Angst et al. 2021) is increasingly recognized as an important pathway of SOM stabilization and may contribute significantly

more to SOM formation under certain conditions (Whalen et al. 2022). We also acknowledge that a major limitation of our microcosm design was the absence of living plants, thus preventing live plant inputs as well as inputs and activities of microbial groups directly associated with plant roots (e.g. ectomycorrhizal fungi, Fernandez and Kennedy 2018). Future studies are needed to track fungal necromass contributions to MAOM formation and chemistry under field conditions with diverse plant communities and more complete soil food webs.

Initial soil microbial properties predicted MAOM formation

We hypothesized that across sites, FeOx concentration and clay content would be strong overall predictors of necromass-derived MAOM formation. While FeOx concentration and clay content were positively correlated with MAOM-C formation for low melanin necromass, we found that initial bacterial community composition most significantly predicted MAOM-C formation. We believe that the strength of this result is likely influenced by the fact that bacterial community composition, as defined by NMDS axes, accounts for variation in soil physicochemical properties. Specifically, we found that bacterial communities with low NMDS1 scores, which explained much of the MAOM-C formation variation, were also associated with higher initial soil FeOx, clay content, and pH. However, MAOM-C formation from high melanin necromass was not related to initial soil physicochemical properties. Previous field studies have shown that melanization increases fungal saprotroph abundances on decaying necromass (Fernandez and Kennedy 2018; Maillard et al. 2023b) and greater relative abundances of soil saprotrophs at the start of our study corresponded with less MAOM-C formation from high melanin necromass after 38 days. Sites with highest fungal saprotroph abundance (C13 and C71) featured increased relative abundances of fast-growing genera such as *Penicillium*, *Ascolobus* and *Umbelopsis*, which were likely targeting necromass polysaccharides (Baldrian et al. 2011; Štursová et al. 2012). Fast growth in fungi is thought to be associated with higher metabolic costs (Arendt 1997; Veresoglou et al. 2018), which may limit microbial transfer of necromass C to MAOM. Given the well-demonstrated potential for melanization to impact decomposer community composition (Fernandez and Kennedy 2018; Maillard et al. 2023b), it would be interesting in future studies to assess how melanin content influences microbial CUE.

In terms of fungal necromass as a source of MAOM-N, we found that soils with greater relative abundances of bacterial copiotrophs formed less necromass derived MAOM-N regardless of necromass type. Copiotrophic bacteria have been regularly shown to be early decomposers of fungal necromass (<35 days; Brabcová et al. 2016; López-Mondéjar et al. 2018; Cantoran et al. 2023; Kennedy and Maillard 2023; Maillard et al. 2023b) and are likely capitalizing on an abundance of labile necromass compounds, including amide-N contained in proteins and chitin (Certano et al. 2018; See et al. 2021). It is

hypothesized that maintenance energy is higher for copiotrophs, resulting in less efficient growth (Roller and Schmidt 2015; Ma et al. 2023), which would potentially limit microbial transfer of N from necromass to MAOM. Support for this possibility was shown in Ma et al. (2023), who found that soil microbial CUE increased with bacterial oligotroph abundance. Currently, however, it is unclear if nitrogen use efficiency might also be lower for copiotrophic taxa. While it is notable that initial microbial parameters outperformed soil physicochemical properties in predicting MAOM formation, we acknowledge that initial microbial community composition, as determined by high throughput sequencing, does not necessarily reflect microbial community composition or activity over the course of the incubation. That said, the recent demonstration of a core bacterial and fungal necrobiome by Cantoran et al. (2023) suggests that the microbial communities present on decaying necromass show notably consistent temporal trends, even across studies conducted in different biomes. As such, we suggest that fungal necromass might serve as a particularly interesting system to test linkages between DOM chemistry, microbial substrate preferences and SOM accumulation, to help quantify how microbial life strategies might relate to soil C and N preservation (Domeignoz-Horta et al. 2021; Zhang et al. 2021).

Conclusions

This study highlights that SOC and SON storage in temperate forest soils is interactively shaped by soil mineralogy, microbial community attributes, and to a lesser extent, fungal necromass chemistry. Contrary to a dominance of abiotic control on fungal necromass C and N persistence, we found that microbial community attributes were stronger predictors of necromass-derived MAOM formation when compared with soil physiochemical properties, including clay and FeOx concentrations. Sites with higher relative abundances of fungal saprotrophs and bacterial copiotrophs at the start of the study formed less fungal necromass derived MAOM after 38 days. Further, we demonstrate the direct potential of fungal cell wall melaninization to influence soluble necromass chemistry and limit mineral associated C accumulation. These findings align with previous studies that report slower decay and microbial assimilation of melanized fungal necromass under field conditions (Fernandez et al. 2016; Maillard et al. 2023b), as well as studies that report greater MAOM formation from high quality plant litter inputs during early stages of decay (Cotrufo and Lavallee 2022). On the whole, our study showed that microbial decomposition decreased the retention of fungal necromass derived-C while increasing the retention of necromass derived-N, highlighting the importance of microbial transformations in the loss of fungal C and preservation of fungal N. While the necromass used in our study had lower chemical and taxonomic complexity than necromass that occurs naturally within soils (Buckeridge et al. 2020), we hope that future

studies can build on our findings by exploring microbial transformations of fungal necromass compounds produced and decayed within their in-situ community context.

Acknowledgments

We thank Joy Gallion the former CFI director at DNR for her help in obtaining the soils used in this study and Brien Beidler for help in fabricating vented microcosm tops. This work was funded by a National Science Foundation DEB MacroSysBIO & NEON-Enabled Science grant (Award# 2106096) and the Department of Energy, Office of Biological and Environmental Research, Genomic Science Program as part of the *Microbes Persist* Soil Microbiome SFA (Award # SCW1632).

References

Angst, G., Mueller, K.E., Nierop, K.G.J., Simpson, M.J., 2021. Plant- or microbial-derived? A review on the molecular composition of stabilized soil organic matter. Soil Biology and Biochemistry 156, 108189. doi:10.1016/j.soilbio.2021.108189

Arendt, J.D., 1997. Adaptive Intrinsic Growth Rates: An Integration Across Taxa. The Quarterly Review of Biology 72, 149–177. doi:10.1086/419764

Artz, R.R.E., Chapman, S.J., Jean Robertson, A.H., Potts, J.M., Laggoun-Défarge, F., Gogo, S., Comont, L., Disnar, J.-R., Francez, A.-J., 2008. FTIR spectroscopy can be used as a screening tool for organic matter quality in regenerating cutover peatlands. Soil Biology and Biochemistry 40, 515–527. doi:10.1016/j.soilbio.2007.09.019

Bailey, V.L., Bond□Lamberty, B., DeAngelis, K., Grandy, A.S., Hawkes, C.V., Heckman, K., Lajtha, K., Phillips, R.P., Sulman, B.N., Todd□Brown, K.E.O., Wallenstein, M.D., 2018. Soil carbon cycling proxies: Understanding their critical role in predicting climate change feedbacks. Global Change Biology 24, 895–905. doi:10.1111/gcb.13926

Baldrian, P., Voříšková, J., Dobiášová, P., Merhautová, V., Lisá, L., Valášková, V., 2011. Production of extracellular enzymes and degradation of biopolymers by saprotrophic microfungi from the upper layers of forest soil. Plant and Soil 338, 111–125. doi:10.1007/s11104-010-0324-3

Beidler, K.V., Phillips, R.P., Andrews, E., Maillard, F., Mushinski, R.M., Kennedy, P.G., 2020. Substrate quality drives fungal necromass decay and decomposer community structure under contrasting vegetation types. Journal of Ecology 108, 1845–1859. doi:10.1111/1365-2745.13385

Bell, A.A., Wheeler, M.H., 1986. Biosynthesis and Functions of Fungal Melanins. Annual Review of Phytopathology 24, 411–451. doi:10.1146/annurev.py.24.090186.002211

Brabcová, V., Nováková, M., Davidová, A., Baldrian, P., 2016. Dead fungal mycelium in forest soil represents a decomposition hotspot and a habitat for a specific microbial community. New Phytologist 210, 1369–1381. doi:10.1111/nph.13849

Brabcová, V., Štursová, M., Baldrian, P., 2018. Nutrient content affects the turnover of fungal biomass in forest topsoil and the composition of associated microbial communities. Soil Biology and Biochemistry 118, 187–198. doi:10.1016/j.soilbio.2017.12.012

Buckeridge, K.M., La Rosa, A.F., Mason, K.E., Whitaker, J., McNamara, N.P., Grant, H.K., Ostle, N.J., 2020. Sticky dead microbes: Rapid abiotic retention of microbial necromass in soil. Soil Biology and Biochemistry 149, 107929. doi:10.1016/j.soilbio.2020.107929

Buckeridge, K.M., Mason, K.E., Ostle, N., McNamara, N.P., Grant, H.K., Whitaker, J., 2022. Microbial necromass carbon and nitrogen persistence are decoupled in agricultural grassland soils. Communications Earth & Environment 3, 114. doi:10.1038/s43247-022-00439-0

Bull, A.T., 1970. Chemical Composition of Wild-type and Mutant Aspergillus nidulans Cell Walls. The Nature of Polysaccharide and Melanin Constituents. Journal of General Microbiology 63, 75–94. doi:10.1099/00221287-63-1-75

Butler, M.J., Day, A.W., 1998. Fungal melanins: a review. Canadian Journal of Microbiology 44, 1115–1136. doi:10.1139/w98-119

Callahan, B.J., McMurdie, P.J., Rosen, M.J., Han, A.W., Johnson, A.J.A., Holmes, S.P., 2016. DADA2: High-resolution sample inference from Illumina amplicon data. Nature Methods 13, 581–583. doi:10.1038/nmeth.3869

Cambardella, C.A., Elliott, E.T., 1992. Particulate Soil Organic Matter Changes across a Grassland Cultivation Sequence. Soil Science Society of America Journal 56, 777–783. doi:10.2136/sssaj1992.03615995005600030017x

Cantoran, A., Maillard, F., Baldrian, P., Kennedy, P.G., 2023. Defining a core microbial necrobiome associated with decomposing fungal necromass. FEMS Microbiology Ecology 99, fiad098. doi:10.1093/femsec/fiad098

Caporaso, J.G., Lauber, C.L., Walters, W.A., Berg-Lyons, D., Huntley, J., Fierer, N., Owens, S.M., Betley, J., Fraser, L., Bauer, M., Gormley, N., Gilbert, J.A., Smith, G., Knight, R., 2012. Ultra-high-throughput microbial community analysis on the Illumina HiSeq and MiSeq platforms. The ISME Journal 6, 1621–1624. doi:10.1038/ismej.2012.8

Certano, A.K., Fernandez, C.W., Heckman, K.A., Kennedy, P.G., 2018. The afterlife effects of fungal morphology: Contrasting decomposition rates between diffuse and rhizomorphic necromass. Soil Biology and Biochemistry 126, 76–81. doi:10.1016/j.soilbio.2018.08.002

Clemmensen, K.E., Bahr, A., Ovaskainen, O., Dahlberg, A., Ekblad, A., Wallander, H., Stenlid, J., Finlay, R.D., Wardle, D.A., Lindahl, B.D., 2013. Roots and Associated Fungi Drive Long-Term Carbon Sequestration in Boreal Forest. Science 339, 1615–1618. doi:10.1126/science.1231923

Comeau, L.-P., Lemke, R.L., Knight, J.D., Bedard-Haughn, A., 2013. Carbon input from 13C-labeled crops in four soil organic matter fractions. Biology and Fertility of Soils 49, 1179–1188. doi:10.1007/s00374-013-0816-4

Cotrufo, M.F., Lavallee, J.M., 2022. Soil organic matter formation, persistence, and functioning: A synthesis of current understanding to inform its conservation and regeneration, in: Advances in Agronomy. Elsevier, pp. 1–66. doi:10.1016/bs.agron.2021.11.002

Cotrufo, M.F., Soong, J.L., Horton, A.J., Campbell, E.E., Haddix, M.L., Wall, D.H., Parton, W.J., 2015. Formation of soil organic matter via biochemical and physical pathways of litter mass loss. Nature Geoscience 8, 776–779. doi:10.1038/ngeo2520

Cotrufo, M.F., Wallenstein, M.D., Boot, C.M., Denef, K., Paul, E., 2013. The Microbial Efficiency□ M atrix Stabilization (MEMS) framework integrates plant litter decomposition with soil organic matter stabilization: do labile plant inputs form stable soil organic matter? Global Change Biology 19, 988–995. doi:10.1111/gcb.12113

Craig, M.E., Geyer, K.M., Beidler, K.V., Brzostek, E.R., Frey, S.D., Stuart Grandy, A., Liang, C., Phillips, R.P., 2022. Fast-decaying plant litter enhances soil carbon in temperate forests but not through microbial physiological traits. Nature Communications 13, 1229. doi:10.1038/s41467-022-28715-9

Deng, Y., Dixon, J.B., 2018. Soil Organic Matter and Organic-Mineral Interactions, in: Dixon, J.B., Schulze, D.G. (Eds.), SSSA Book Series. Soil Science Society of America, Madison, WI, USA, pp. 69–107. doi:10.2136/sssabookser7.c3

Domeignoz-Horta, L.A., Shinfuku, M., Junier, P., Poirier, S., Verrecchia, E., Sebag, D., DeAngelis, K.M., 2021. Direct evidence for the role of microbial community composition in the formation of soil organic matter composition and persistence. ISME Communications 1, 64. doi:10.1038/s43705-021-00071-7

Drever, M.C., Douglas, T.J., Domalik, A.D., Balke, E., Scott, D.C., Johnson, M.S., Gurd, D.B., 2023. Water diversion structures and river discharge dictate salinity dynamics on tidal flats of the Fraser River delta, British Columbia. Estuarine, Coastal and Shelf Science 291, 108436. doi:10.1016/j.ecss.2023.108436

Dzurendova, S., Zimmermann, B., Kohler, A., Tafintseva, V., Slany, O., Certik, M., Shapaval, V., 2020. Microcultivation and FTIR spectroscopy-based screening revealed a nutrient-induced co-

production of high-value metabolites in oleaginous Mucoromycota fungi. PLOS ONE 15, e0234870. doi:10.1371/journal.pone.0234870

Egli, M., Mirabella, A., Kägi, B., Tomasone, R., Colorio, G., 2006. Influence of steam sterilisation on soil chemical characteristics, trace metals and clay mineralogy. Geoderma 131, 123–142. doi:10.1016/j.geoderma.2005.03.017

Ellerbrock, R.H., Kaiser, M., 2005. Stability and composition of different soluble soil organic matter fractions–evidence from δ13C and FTIR signatures. Geoderma 128, 28–37. doi:10.1016/j.geoderma.2004.12.025

Fehrer, J., Réblová, M., Bambasová, V., Vohník, M., 2019. The root-symbiotic *Rhizoscyphus ericae* aggregate and *Hyaloscypha* (*Leotiomycetes*) are congeneric: Phylogenetic and experimental evidence. Studies in Mycology 92, 195–225. doi:10.1016/j.simyco.2018.10.004

Fernandez, C.W., Heckman, K., Kolka, R., Kennedy, P.G., 2019. Melanin mitigates the accelerated decay of mycorrhizal necromass with peatland warming. Ecology Letters 22, 498–505. doi:10.1111/ele.13209

Fernandez, C.W., Kennedy, P.G., 2018. Melanization of mycorrhizal fungal necromass structures microbial decomposer communities. Journal of Ecology 106, 468–479. doi:10.1111/1365-2745.12920

Fernandez, C.W., Koide, R.T., 2014. Initial melanin and nitrogen concentrations control the decomposition of ectomycorrhizal fungal litter. Soil Biology and Biochemistry 77, 150–157. doi:10.1016/j.soilbio.2014.06.026

Fernandez, C.W., Koide, R.T., 2012. The role of chitin in the decomposition of ectomycorrhizal fungal litter. Ecology 93, 24–28. doi:10.1890/11-1346.1

Fernandez, C.W., Langley, J.A., Chapman, S., McCormack, M.L., Koide, R.T., 2016. The decomposition of ectomycorrhizal fungal necromass. Soil Biology and Biochemistry 93, 38–49. doi:10.1016/j.soilbio.2015.10.017

Fierer, N., Schimel, J.P., 2002. Effects of drying–rewetting frequency on soil carbon and nitrogen transformations. Soil Biology and Biochemistry 34, 777–787. doi:10.1016/S0038-0717(02)00007-X

Frey, S.D., 2019. Mycorrhizal Fungi as Mediators of Soil Organic Matter Dynamics. Annual Review of Ecology, Evolution, and Systematics 50, 237–259. doi:10.1146/annurev-ecolsys-110617-062331

Godbold, D.L., Hoosbeek, M.R., Lukac, M., Cotrufo, M.F., Janssens, I.A., Ceulemans, R., Polle, A., Velthorst, E.J., Scarascia-Mugnozza, G., De Angelis, P., Miglietta, F., Peressotti, A., 2006. Mycorrhizal Hyphal Turnover as a Dominant Process for Carbon Input into Soil Organic Matter. Plant and Soil 281, 15–24. doi:10.1007/s11104-005-3701-6

Golchin, A., Clarke, P., Oades, J.M., 1996. The heterogeneous nature of microbial products as shown by solid-state13C CP/MAS NMR spectroscopy. Biogeochemistry 34, 71–97. doi:10.1007/BF02180974

Goldberg, S., Kapoor, B.S., Rhoades, J.D., 1990. Effect of aluminum and iron oxides and organic matter on flocculation and dispersion of arid zone soils: Soil Science 150, 588–593. doi:10.1097/00010694-199009000-00004

Grelet, G., Johnson, D., Paterson, E., Anderson, I.C., Alexander, I.J., 2009. Reciprocal carbon and nitrogen transfer between an ericaceous dwarf shrub and fungi isolated from *Piceirhiza bicolorata* ectomycorrhizas. New Phytologist 182, 359–366. doi:10.1111/j.1469-8137.2009.02813.x

Harsh, J., Chorover, J., Nizeyimana, E., 2018. Allophane and Imogolite, in: Dixon, J.B., Schulze, D.G. (Eds.), SSSA Book Series. Soil Science Society of America, Madison, WI, USA, pp. 291–322. doi:10.2136/sssabookser7.c9

Hu, Y., Zheng, Q., Noll, L., Zhang, S., Wanek, W., 2020. Direct measurement of the in situ decomposition of microbial-derived soil organic matter. Soil Biology and Biochemistry 141, 107660. doi:10.1016/j.soilbio.2019.107660

Jagadamma, S., Mayes, M.A., Phillips, J.R., 2012. Selective Sorption of Dissolved Organic Carbon Compounds by Temperate Soils. PLoS ONE 7, e50434. doi:10.1371/journal.pone.0050434

Kalbitz, K., Schwesig, D., Rethemeyer, J., Matzner, E., 2005. Stabilization of dissolved organic matter by sorption to the mineral soil. Soil Biology and Biochemistry 37, 1319–1331. doi:10.1016/j.soilbio.2004.11.028

Kallenbach, C.M., Frey, S.D., Grandy, A.S., 2016. Direct evidence for microbial-derived soil organic matter formation and its ecophysiological controls. Nature Communications 7, 13630. doi:10.1038/ncomms13630

Kennedy, P.G., Maillard, F., 2023. Knowns and unknowns of the soil fungal necrobiome. Trends in Microbiology 31, 173–180. doi:10.1016/j.tim.2022.08.011

Kleber, M., Eusterhues, K., Keiluweit, M., Mikutta, C., Mikutta, R., Nico, P.S., 2015. Mineral–Organic Associations: Formation, Properties, and Relevance in Soil Environments, in: Advances in Agronomy. Elsevier, pp. 1–140. doi:10.1016/bs.agron.2014.10.005

Kleber, M., Sollins, P., Sutton, R., 2007. A conceptual model of organo-mineral interactions in soils: self-assembly of organic molecular fragments into zonal structures on mineral surfaces. Biogeochemistry 85, 9–24. doi:10.1007/s10533-007-9103-5

Kögel-Knabner, I., 2002. The macromolecular organic composition of plant and microbial residues as inputs to soil organic matter. Soil Biology and Biochemistry 34, 139–162. doi:10.1016/S0038-0717(01)00158-4

Krumina, L., Lyngsie, G., Tunlid, A., Persson, P., 2017. Oxidation of a Dimethoxyhydroquinone by Ferrihydrite and Goethite Nanoparticles: Iron Reduction versus Surface Catalysis. Environmental Science & Technology 51, 9053–9061. doi:10.1021/acs.est.7b02292

Langseter, A.M., Dzurendova, S., Shapaval, V., Kohler, A., Ekeberg, D., Zimmermann, B., 2021. Evaluation and optimisation of direct transesterification methods for the assessment of lipid accumulation in oleaginous filamentous fungi. Microbial Cell Factories 20, 59. doi:10.1186/s12934-021-01542-1

Lehmann, J., Hansel, C.M., Kaiser, C., Kleber, M., Maher, K., Manzoni, S., Nunan, N., Reichstein, M., Schimel, J.P., Torn, M.S., Wieder, W.R., Kögel-Knabner, I., 2020. Persistence of soil organic carbon caused by functional complexity. Nature Geoscience 13, 529–534. doi:10.1038/s41561-020-0612-3

Lehmann, J., Kleber, M., 2015. The contentious nature of soil organic matter. Nature 528, 60–68. doi:10.1038/nature16069

Lenth, R. (2022). emmeans: Estimated marginal means, aka least-squares means. R package

Liang, C., Amelung, W., Lehmann, J., Kästner, M., 2019. Quantitative assessment of microbial necromass contribution to soil organic matter. Global Change Biology 25, 3578–3590. doi:10.1111/gcb.14781

Liang, C., Schimel, J.P., Jastrow, J.D., 2017. The importance of anabolism in microbial control over soil carbon storage. Nature Microbiology 2, 17105. doi:10.1038/nmicrobiol.2017.105

López-Mondéjar, R., Brabcová, V., Štursová, M., Davidová, A., Jansa, J., Cajthaml, T., Baldrian, P., 2018. Decomposer food web in a deciduous forest shows high share of generalist microorganisms and importance of microbial biomass recycling. The ISME Journal 12, 1768–1778. doi:10.1038/s41396-018-0084-2

Lützow, M.V., Kögel□Knabner, I., Ekschmitt, K., Matzner, E., Guggenberger, G., Marschner, B., Flessa, H., 2006. Stabilization of organic matter in temperate soils: mechanisms and their relevance under different soil conditions – a review. European Journal of Soil Science 57, 426–445. doi:10.1111/j.1365-2389.2006.00809.x

Ma, S., Zhu, W., Wang, W., Li, X., Sheng, Z., 2023. Microbial assemblies with distinct trophic strategies drive changes in soil microbial carbon use efficiency along vegetation primary succession in a glacier retreat area of the southeastern Tibetan Plateau. Science of The Total Environment 867, 161587. doi:10.1016/j.scitotenv.2023.161587

Maillard, F., Beatty, B., Park, M., Adamczyk, S., Adamczyk, B., See, C.R., Cavender-Bares, J., Hobbie, S.E., Kennedy, P.G., 2023a. Microbial community attributes supersede plant and soil parameters in predicting fungal necromass decomposition rates in a 12-tree species common garden experiment. Soil Biology and Biochemistry 184, 109124. doi:10.1016/j.soilbio.2023.109124

Maillard, F., Michaud, T.J., See, C.R., DeLancey, L.C., Blazewicz, S.J., Kimbrel, J.A., Pett-Ridge, J., Kennedy, P.G., 2023b. Melanization slows the rapid movement of fungal necromass carbon and nitrogen into both bacterial and fungal decomposer communities and soils. mSystems e00390-23. doi:10.1128/msystems.00390-23

Maillard, F., Pflender, S., Heckman, K.A., Chalot, M., Kennedy, P.G., 2023c. Fungal necromass presents a high potential for Mercury immobilization in soil. Chemosphere 311, 136994. doi:10.1016/j.chemosphere.2022.136994

Maillard, F., Schilling, J., Andrews, E., Schreiner, K.M., Kennedy, P., 2020. Functional convergence in the decomposition of fungal necromass in soil and wood. FEMS Microbiology Ecology 96, fiz209. doi:10.1093/femsec/fiz209

Manzoni, S., Čapek, P., Porada, P., Thurner, M., Winterdahl, M., Beer, C., Brüchert, V., Frouz, J., Herrmann, A.M., Lindahl, B.D., Lyon, S.W., Šantrůčková, H., Vico, G., Way, D., 2018. Reviews and syntheses: Carbon use efficiency from organisms to ecosystems – definitions, theories, and empirical evidence. Biogeosciences 15, 5929–5949. doi:10.5194/bg-15-5929-2018

Matus, F.J., 2021. Fine silt and clay content is the main factor defining maximal C and N accumulations in soils: a meta-analysis. Scientific Reports 11, 6438. doi:10.1038/s41598-021-84821-6

Mikutta, R., Mikutta, C., Kalbitz, K., Scheel, T., Kaiser, K., Jahn, R., 2007. Biodegradation of forest floor organic matter bound to minerals via different binding mechanisms. Geochimica et Cosmochimica Acta 71, 2569–2590. doi:10.1016/j.gca.2007.03.002

Miltner, A., Kindler, R., Knicker, H., Richnow, H.-H., Kästner, M., 2009. Fate of microbial biomass-derived amino acids in soil and their contribution to soil organic matter. Organic Geochemistry 40, 978–985. doi:10.1016/j.orggeochem.2009.06.008

Minasny, B., Malone, B.P., McBratney, A.B., Angers, D.A., Arrouays, D., Chambers, A., Chaplot, V., Chen, Z.-S., Cheng, K., Das, B.S., Field, D.J., Gimona, A., Hedley, C.B., Hong, S.Y., Mandal, B., Marchant, B.P., Martin, M., McConkey, B.G., Mulder, V.L., O'Rourke, S., Richer-de-Forges, A.C., Odeh, I., Padarian, J., Paustian, K., Pan, G., Poggio, L., Savin, I., Stolbovoy, V., Stockmann, U., Sulaeman, Y., Tsui, C.-C., Vågen, T.-G., Van Wesemael, B., Winowiecki, L., 2017. Soil carbon 4 per mille. Geoderma 292, 59–86. doi:10.1016/j.geoderma.2017.01.002

Norén, K., Loring, J.S., Persson, P., 2008. Adsorption of alpha amino acids at the water/goethite interface. Journal of Colloid and Interface Science 319, 416–428. doi:10.1016/j.jcis.2007.11.046

Nguyen, N.H., Song, Z., Bates, S.T., Branco, S., Tedersoo, L., Menke, J., Schilling, J.S., Kennedy, P.G., 2016. FUNGuild: An open annotation tool for parsing fungal community datasets by ecological guild. Fungal Ecology 20, 241–248. doi:10.1016/j.funeco.2015.06.006

Omoike, A., Chorover, J., 2006. Adsorption to goethite of extracellular polymeric substances from Bacillus subtilis. Geochimica et Cosmochimica Acta 70, 827–838. doi:10.1016/j.gca.2005.10.012

Oksanen J., Blanchet F. G., Kindt R., Legendre P., Minchin P. R., O'Hara R. B., et al. (2022). vegan: Community Ecology Package. R package version 2.6-4.

Palmer, J.M., Jusino, M.A., Banik, M.T., Lindner, D.L., 2018. Non-biological synthetic spike-in controls and the AMPtk software pipeline improve mycobiome data. PeerJ 6, e4925. doi:10.7717/peerj.4925

Pärnpuu, S., Astover, A., Tõnutare, T., Penu, P., Kauer, K., 2022. Soil organic matter qualification with FTIR spectroscopy under different soil types in Estonia. Geoderma Regional 28, e00483. doi:10.1016/j.geodrs.2022.e00483

Põlme, S., Abarenkov, K., Henrik Nilsson, R., Lindahl, B.D., Clemmensen, K.E., Kauserud, H., Nguyen, N., Kjøller, R., Bates, S.T., Baldrian, P., Frøslev, T.G., Adojaan, K., Vizzini, A., Suija, A., Pfister, D., Baral, H.-O., Järv, H., Madrid, H., Nordén, J., Liu, J.-K., Pawlowska, J., Põldmaa, K., Pärtel, K., Runnel, K., Hansen, K., Larsson, K.-H., Hyde, K.D., Sandoval-Denis, M., Smith, M.E., Toome-Heller, M., Wijayawardene, N.N., Menolli, N., Reynolds, N.K., Drenkhan, R., Maharachchikumbura, S.S.N., Gibertoni, T.B., Læssøe, T., Davis, W., Tokarev, Y., Corrales, A., Soares, A.M., Agan, A., Machado, A.R., Argüelles-Moyao, A., Detheridge, A., De Meiras-Ottoni, A., Verbeken, A., Dutta, A.K., Cui, B.-K., Pradeep, C.K., Marín, C., Stanton, D., Gohar, D., Wanasinghe, D.N., Otsing, E., Aslani, F., Griffith, G.W., Lumbsch, T.H., Grossart, H.-P., Masigol, H., Timling, I., Hiiesalu, I., Oja, J., Kupagme, J.Y., Geml, J., Alvarez-Manjarrez, J., Ilves, K., Loit, K., Adamson, K., Nara, K., Küngas, K., Rojas-Jimenez, K., Bitenieks, K., Irinyi, L., Nagy, L.G., Soonvald, L., Zhou, L.-W., Wagner, L., Aime, M.C., Öpik, M., Mujica, M.I., Metsoja, M., Ryberg, M., Vasar, M., Murata, M., Nelsen, M.P., Cleary, M., Samarakoon, M.C., Doilom, M., Bahram, M., Hagh-Doust, N., Dulya, O., Johnston, P., Kohout, P., Chen, Q., Tian, Q., Nandi, R., Amiri, R., Perera, R.H., Dos Santos Chikowski, R., Mendes-Alvarenga, R.L., Garibay-Orijel, R., Gielen, R., Phookamsak, R., Jayawardena, R.S., Rahimlou, S., Karunarathna, S.C., Tibpromma, S., Brown, S.P., Sepp, S.-K., Mundra, S., Luo, Z.-H., Bose, T., Vahter, T., Netherway, T., Yang, T., May, T., Varga, T., Li, W., Coimbra, V.R.M., De Oliveira, V.R.T., De Lima, V.X., Mikryukov, V.S., Lu, Y., Matsuda, Y., Miyamoto, Y., Kõljalg, U., Tedersoo, L., 2020. FungalTraits: a user-friendly traits database of fungi and fungus-like stramenopiles. Fungal Diversity 105, 1–16. doi:10.1007/s13225-020-00466-2

Rasmussen, C., Heckman, K., Wieder, W.R., Keiluweit, M., Lawrence, C.R., Berhe, A.A., Blankinship, J.C., Crow, S.E., Druhan, J.L., Hicks Pries, C.E., Marin-Spiotta, E., Plante, A.F., Schädel, C., Schimel, J.P., Sierra, C.A., Thompson, A., Wagai, R., 2018. Beyond clay: towards an improved set of variables for predicting soil organic matter content. Biogeochemistry 137, 297–306. doi:10.1007/s10533-018-0424-3

Rillig, M.C., Caldwell, B.A., Wösten, H.A.B., Sollins, P., 2007. Role of proteins in soil carbon and nitrogen storage: controls on persistence. Biogeochemistry 85, 25–44. doi:10.1007/s10533-007-9102-6

Roller, B.R.K., Schmidt, T.M., 2015. The physiology and ecological implications of efficient growth. The ISME Journal 9, 1481–1487. doi:10.1038/ismej.2014.235

Ross, R.L. and Wang, C., 1993.Extractable Al, Fe, Mn and Si," In: M. R. Carter, Ed., Soil Sampling and Methods of Analysis, Lewis Publication, Boca Raton, pp. 239-246.

Ryan, M.E., Schreiner, K.M., Swenson, J.T., Gagne, J., Kennedy, P.G., 2020. Rapid changes in the chemical composition of degrading ectomycorrhizal fungal necromass. Fungal Ecology 45, 100922. doi:10.1016/j.funeco.2020.100922

Schweigert, M., Herrmann, S., Miltner, A., Fester, T., Kästner, M., 2015. Fate of ectomycorrhizal fungal biomass in a soil bioreactor system and its contribution to soil organic matter formation. Soil Biology and Biochemistry 88, 120–127. doi:10.1016/j.soilbio.2015.05.012

See, C.R., Fernandez, C.W., Conley, A.M., DeLancey, L.C., Heckman, K.A., Kennedy, P.G., Hobbie, S.E., 2021. Distinct carbon fractions drive a generalisable two-pool model of fungal necromass decomposition. Functional Ecology 35, 796–806. doi:10.1111/1365-2435.13728

See, C.R., Keller, A.B., Hobbie, S.E., Kennedy, P.G., Weber, P.K., Pett□Ridge, J., 2022. Hyphae move matter and microbes to mineral microsites: Integrating the hyphosphere into conceptual models of soil organic matter stabilization. Global Change Biology 28, 2527–2540. doi:10.1111/gcb.16073

Simpson, A.J., Simpson, M.J., Smith, E., Kelleher, B.P., 2007b. Microbially Derived Inputs to Soil Organic Matter: Are Current Estimates Too Low? Environmental Science & Technology 41, 8070–8076. doi:10.1021/es071217x

Siletti, C.E., Zeiner, C.A., Bhatnagar, J.M., 2017. Distributions of fungal melanin across species and soils. Soil Biology and Biochemistry 113, 285–293. doi:10.1016/j.soilbio.2017.05.030

Sokol, N.W., Bradford, M.A., 2019. Microbial formation of stable soil carbon is more efficient from belowground than aboveground input. Nature Geoscience 12, 46–53. doi:10.1038/s41561-018-0258-6

Sollins, P., Homann, P., Caldwell, B.A., 1996. Stabilization and destabilization of soil organic matter: mechanisms and controls. Geoderma 74, 65–105. doi:10.1016/S0016-7061(96)00036-5

Stuart, B.H., 2004. Infrared Spectroscopy: Fundamentals and Applications, 1st ed, Analytical Techniques in the Sciences. Wiley. doi:10.1002/0470011149

Štursová, M., Žifčáková, L., Leigh, M.B., Burgess, R., Baldrian, P., 2012. Cellulose utilization in forest litter and soil: identification of bacterial and fungal decomposers. FEMS Microbiology Ecology 80, 735–746. doi:10.1111/j.1574-6941.2012.01343.x

Sulman, B.N., Phillips, R.P., Oishi, A.C., Shevliakova, E., Pacala, S.W., 2014. Microbe-driven turnover offsets mineral-mediated storage of soil carbon under elevated CO2. Nature Climate Change 4, 1099–1102. doi:10.1038/nclimate2436

Taylor, D.L., Walters, W.A., Lennon, N.J., Bochicchio, J., Krohn, A., Caporaso, J.G., Pennanen, T., 2016. Accurate Estimation of Fungal Diversity and Abundance through Improved Lineage-Specific Primers Optimized for Illumina Amplicon Sequencing. Applied and Environmental Microbiology 82, 7217–7226. doi:10.1128/AEM.02576-16

Theng, B.K.G., 2024. The Chemistry of Clay-Organic Reactions, 2nd ed. CRC Press, Boca Raton. doi:10.1201/9781003080244

Tian, Z., Wang, T., Tunlid, A., Persson, P., 2020. Proteolysis of Iron Oxide-Associated Bovine Serum Albumin. Environmental Science & Technology 54, 5121–5130. doi:10.1021/acs.est.0c00860

Trivedi, P., Delgado□Baquerizo, M., Jeffries, T.C., Trivedi, C., Anderson, I.C., Lai, K., McNee, M., Flower, K., Pal Singh, B., Minkey, D., Singh, B.K., 2017. Soil aggregation and associated microbial communities modify the impact of agricultural management on carbon content. Environmental Microbiology 19, 3070–3086. doi:10.1111/1462-2920.13779

Van Der Wal, A., Bloem, J., Mulder, C., De Boer, W., 2009. Relative abundance and activity of melanized hyphae in different soil ecosystems. Soil Biology and Biochemistry 41, 417–419. doi:10.1016/j.soilbio.2008.10.031

Villacís-García, M., Ugalde-Arzate, M., Vaca-Escobar, K., Villalobos, M., Zanella, R., Martínez-Villegas, N., 2015. Laboratory synthesis of goethite and ferrihydrite of controlled particle sizes. Boletín de la Sociedad Geológica Mexicana 67, 433-446.

Veresoglou, S.D., Rillig, M.C., Johnson, D., 2018. Responsiveness of plants to mycorrhiza regulates coexistence. Journal of Ecology 106, 1864–1875. doi:10.1111/1365-2745.13026

Wang, B., An, S., Liang, C., Liu, Y., Kuzyakov, Y., 2021. Microbial necromass as the source of soil organic carbon in global ecosystems. Soil Biology and Biochemistry 162, 108422. doi:10.1016/j.soilbio.2021.108422

Wang, C., Kuzyakov, Y., 2024. Soil organic matter priming: The pH effects. Global Change Biology 30, e17349. doi:10.1111/gcb.17349

Wang, C., Wang, X., Pei, G., Xia, Z., Peng, B., Sun, L., Wang, J., Gao, D., Chen, S., Liu, D., Dai, W., Jiang, P., Fang, Y., Liang, C., Wu, N., Bai, E., 2020. Stabilization of microbial residues in soil organic matter after two years of decomposition. Soil Biology and Biochemistry 141, 107687. doi:10.1016/j.soilbio.2019.107687

Wang, Q., Cole, J.R., 2024. Updated RDP taxonomy and RDP Classifier for more accurate taxonomic classification. Microbiology Resource Announcements 13, e01063-23. doi:10.1128/mra.01063-23

Wang, Xu, Wang, C., Fan, X., Sun, L., Sang, C., Wang, Xugao, Jiang, P., Fang, Y., Bai, E., 2024. Mineral composition controls the stabilization of microbially derived carbon and nitrogen in soils: Insights from an isotope tracing model. Global Change Biology 30, e17156. doi:10.1111/gcb.17156

Warren, C., 2021. What are the products of enzymatic cleavage of organic N? Soil Biology and Biochemistry 154, 108152. doi:10.1016/j.soilbio.2021.108152

Whalen, E.D., Grandy, A.S., Sokol, N.W., Keiluweit, M., Ernakovich, J., Smith, R.G., Frey, S.D., 2022. Clarifying the evidence for microbial□ and plant□derived soil organic matter, and the path toward a more quantitative understanding. Global Change Biology 28, 7167–7185. doi:10.1111/gcb.16413

Wieder, W.R., Grandy, A.S., Kallenbach, C.M., Bonan, G.B., 2014. Integrating microbial physiology and physio-chemical principles in soils with the MIcrobial-MIneral Carbon Stabilization (MIMICS) model. Biogeosciences 11, 3899–3917. doi:10.5194/bg-11-3899-2014

Wu, S., Konhauser, K.O., Chen, B., Huang, L., 2023. “Reactive Mineral Sink” drives soil organic matter dynamics and stabilization. Npj Materials Sustainability 1, 3. doi:10.1038/s44296-023-00003-7

Zhang, S., Fang, Y., Luo, Y., Li, Yongchun, Ge, T., Wang, Y., Wang, H., Yu, B., Song, X., Chen, J., Zhou, J., Li, Yongfu, Chang, S.X., 2021. Linking soil carbon availability, microbial community composition and enzyme activities to organic carbon mineralization of a bamboo forest soil amended with pyrogenic and fresh organic matter. Science of The Total Environment 801, 149717. doi:10.1016/j.scitotenv.2021.149717

Supplemental Information

Table S1. Initial necromass chemistry (mean, SD, n = 3) for high and low melanin *Hyaloscypha bicolor* necromass types before (non-sterile) and after autoclaving (sterile).

Necromass Type	High Melanin		Low Melanin	
Initial	Non-Sterile	Sterile*	Non-Sterile	Sterile*
% C	43.3 (1.3)[a]	48.2 (9.9)[a]	51.4 (0.33)[b]	48.3 (0.90)[c]
% N	3.28 (0.18)[a]	3.94 (0.61)[a]	3.93 (0.06)[a]	3.62 (0.11)[a]
‰ $\delta^{13}C$	31.4 (1.2)[a]	31.7 (1.3)[a]	35.5 (0.90)[b]	36.39 (0.36)[b]
‰ $\delta^{15}N$	680.4 (21)[a]	849.6 (140)[a]	731.8 (23)[a]	728.8 (8.1)[a]
% Soluble fraction	76.2 (1.2)[a]	----------	77.1 (7.5)[a]	----------
% Acid unhydrolyzable fraction	18.1 (3.4)[a]	----------	16.7 (4.1)[a]	----------

*Sterile necromass was added to sterile soil microcosms in 38-day necromass incubations. There was not enough initial autoclaved necromass available to measure initial C quality fractions.

Table S2. Site locations and overstory tree species for Indiana Department of Natural Resources (IDNR) Continuous Forest Inventory (CFI) plots selected for soil collection.

Latitude	Longitude	Site ID	County	Plot Id	Sampling Date	Tree Species
38.979306	-87.255861	C153	Sullivan	1619	6/5/20	*Pinus virginiana* & *Robinia pseudoacacia*
38.988417	-87.230556	C55	Greene	1601	6/1/20	*Acer rubrum, Asimina triloba, Cornus florida, Morus rubra, Prunus serotina,* & *Quercus ellipsoidalis*
40.812436	-85.714392	C169	Wabash	13	5/21/20	*Celtis occidentalis, Morus alba, Pinus resinosa, Prunus serotina, Quercus muehlenbergii,* & *Ulmus americana*
38.801075	-86.056	C71	Jackson	1859	5/22/20	*Acer saccharum, Paulownia tomentosa,* & *Liriodendron tulipifera*
39.238972	-86.314778	C13	Brown	856	5/26/20	*Acer rubrum, Acer saccharum, Fagus grandifolia, Sassafras albidum,* & *Quercus velutina*
38.170672	-86.252908	C61	Harrison	3667	7/24/20	*Acer saccharum, Nyssa sylvatica,* & *Quercus alba*

Table S3. Peak annotations for diffuse reflectance infrared Fourier transform spectroscopy (DRIFTS).

Wavenumber (cm^{-1})	Peak ID Number	Functional Group	Potential Compound	Alternative Functional Group	Alternative Compound
3695	1	O-H	Clay, minerals	Al-OH	Aluminum, minerals
3650	2	O-H	Clay, minerals	Al-OH	Aluminum, minerals
3621	3	O-H	Clay, minerals	Al-OH	Aluminum, minerals
1683	4	C=O	Carboxylic acids	C=O	Proteins
1609	5	C=C	Aromatic	N-H	Proteins
1521	6	C=C	Aromatic		
1493	7	C=C	Aromatic	N-H	Proteins
1384	8	C-H	Aromatic	C-H	Phenolic
1284	9	C-O	Phenolic		
1159	10	C-O	Polysaccharides	Si-O	Silicate, minerals
1104	11	C-O	Polysaccharides	Si-O	Silicate, minerals
1033	12	C-O	Polysaccharides	Si-O	Silicate, minerals
1013	13	C-O	Polysaccharides	Si-O	Silicate, minerals
940	14	C-H	Aromatic	C-H	Alkenes
916	15	C-H	Aromatic	C-H	Alkenes
798	16	C-H	Aromatic	C-H	Alkenes
779	17	C-H	Aromatic	C-H	Alkenes
695	18	Si-O	Silicate, minerals		
647	19	Si-O	Silicate, minerals		
528	20	Si-O	Silicate, minerals		
474	21	Si-O	Silicate, minerals		

Table S4. Alpha diversity metrics and functional group relative abundances for initial soils (mean, SD, n = 3*). Letters denote differences in site means as determined by ANOVA.

Site ID	Number of Unique Bacterial OTUs	Number of Unique Fungal OTUs	Bacterial Shannon Diversity	Fungal Shannon Diversity	Bacterial Copiotroph Richness	Bacterial Copiotroph Relative Abundance	Bacterial Oligotroph Richness	Bacterial Oligotroph Relative Abundance	Fungal Saprotroph Richness	Fungal Saprotroph Relative Abundance
C153	298 (53)^{a}	115 (28)^{a}	4.91 (0.16)^{a}	4.03 (0.03)^{ab}	63.7 (16)^{a}	0.237 (0.014)^{a}	56.7 (7.2)^{a}	0.245 (0.009)^{a}	42.0 (14)^{a}	0.369 (0.042)
C55	244 (74)^{ab}	252 (18)^{b}	4.27 (0.21)^{b}	4.08 (0.06)^{ab}	33.0 (7.1)^{b}	0.111 (0.033)^{b}	30.5 (6.4)^{b}	0.061 (0.015)^{b}	75.3 (2.1)^{bc}	0.298 (0.074)
C169	201 (61)^{ab}	265 (24)^{b}	4.27 (0.28)^{b}	3.65 (0.18)^{bc}	51.0 (14)^{ab}	0.243 (0.006)^{a}	30.5 (9.2)^{b}	0.115 (0.007)^{c}	85.7 (16)^{c}	0.262 (0.053)
C71	187 (28)^{ab}	260 (20)^{b}	3.89 (0.19)^{b}	4.39 (0.04)^{a}	39.7 (3.1)^{ab}	0.280 (0.028)^{ac}	27.0 (5.0)^{b}	0.060 (0.016)^{b}	91.5 (7.8)^{c}	0.613 (0.030)
C13	154 (13)^{b}	134 (24)^{a}	3.94 (0.09)^{b}	2.88 (0.30)^{d}	35.0 (3.0)^{b}	0.350 (0.022)^{c}	22.3 (2.1)^{b}	0.059 (0.017)^{b}	41.3 (2.1)^{a}	0.579 (0.059)
C61	205 (8.0)^{ab}	162 (10)^{a}	4.32 (0.06)^{b}	3.31 (0.15)^{cd}	41.7 (31)^{ab}	0.261 (0.033)^{a}	31.3 (3.2)^{b}	0.062 (0.006)^{b}	55.3 (9.3)^{ab}	0.374 (0.033)

*****Due to some initial soil samples not passing quality control (see methods), n=2 for sites C55 and C169 for bacterial metrics & n=2 for sites C71 and C153 for fungal metrics.

Table S5. ANOVA table for fungal necromass derived mineral associated organic matter (MAOM) carbon (C) and nitrogen (N) formation in live soil microcosms.

Necromass Derived:	MAOM-C				MAOM-N			
Factor	Df	F	p	Variance Explained (%)	Df	F	p	Variance Explained (%)
Site	5	8.39	<0.001	52.01	5	3.04	0.03	34.6
Necromass Type	1	8.09	0.009	10.03	1	3.85	0.06	8.77
Site x Necro Type	5	1.32	0.29	8.20	5	0.175	0.97	1.99

Table S6. Site means and standard deviations for fungal necromass derived mineral associated organic matter (MAOM) carbon (C) and nitrogen (N) formation in live soil microcosms. Letters denote differences in site means as determined by ANOVA.

Site ID	Fungal Derived MAOM-C (% initial necromass C)	Fungal Derived MAOM-N (% initial necromass N)
C153	6.92 (1.1)[a]	40.1 (4.2)[ab]
C55	6.12 (0.72)[ab]	48.0 (5.9)[a]
C169	5.82 (0.48)[ab]	44.5 (3.5)[ab]
C71	4.41 (0.88)[b]	36.7 (9.7)[b]
C13	5.36 (0.45)[c]	40.6 (2.6)[ab]
C61	5.83 (0.94)[ab]	39.6 (4.3)[ab]

Table S7. ANOVA table for fungal necromass derived mineral associated organic matter (MAOM) carbon (C) and nitrogen (N) formation in sterile and live soil microcosms from sites C153, C169, and C61.

Necromass Derived:	MAOM-C				MAOM-N			
Factor	Df	F	p	Variance Explained (%)	Df	F	p	Variance Explained (%)
Site	2	7.74	0.003	15.9	2	2.78	0.08	8.10
Necromass Type	1	0.527	0.48	0.541	1	2.46	0.130	3.59
Sterilization Treatment	1	47.8	<0.001	49.1	1	32.0	<0.001	46.6
Site x Necro Type	2	0.835	0.45	1.71	2	1.09	0.35	3.19
Site x Ster Treat	2	2.58	0.10	5.29	2	0.166	0.85	0.484
Necro Type x Ster Treat	1	0.793	0.38	0.81	1	0.00	0.99	0.0002
Site x Necro Type x Ster Treat	2	1.01	0.38	2.07	2	1.04	0.37	3.04

Table S8. Necromass derived mineral associated organic matter (MAOM) carbon (C) and nitrogen (N) formation (mean, SD, n = 3) in sterile and live soil microcosms from microcosm subset.

Site ID	Sterilization Treatment	Necromass Type	Fungal Derived MAOM-C (% initial necromass C)	Fungal Derived MAOM-N (% initial necromass N)
C153	Live	High Melanin	6.01 (0.52)	37.6 (4.3)
		Low Melanin	7.82 (0.62)	42.6 (2.4)
	Sterile	High Melanin	11.7 (2.8)	30.2 (7.5)
		Low Melanin	11.5 (3.4)	30.2 (7.6)
C169	Live	High Melanin	5.78 (0.06)	42.6 (3.3)
		Low Melanin	5.85 (0.44)	46.4 (3.0)
	Sterile	High Melanin	7.92 (0.86)	28.5 (1.9)
		Low Melanin	6.87 (1.1)	39.1 (4.1)
C61	Live	High Melanin	5.80 (1.4)	38.8 (6.6)
		Low Melanin	5.85 (0.32)	40.4 (0.87)
	Sterile	High Melanin	9.71 (3.1)	29.3 (9.5)
		Low Melanin	10.9 (0.23)	26.9 (0.24)

A. B.

Figure S1. A. Soil microcosm design with modified vented caps and B. sterile soil microcosm receiving a sterile water addition.

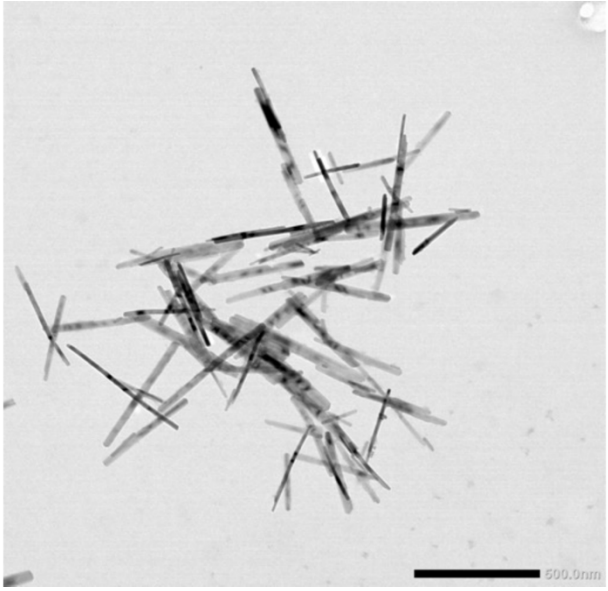

Figure S2. Morphology of goethite under Transmission Electron Microscopy.

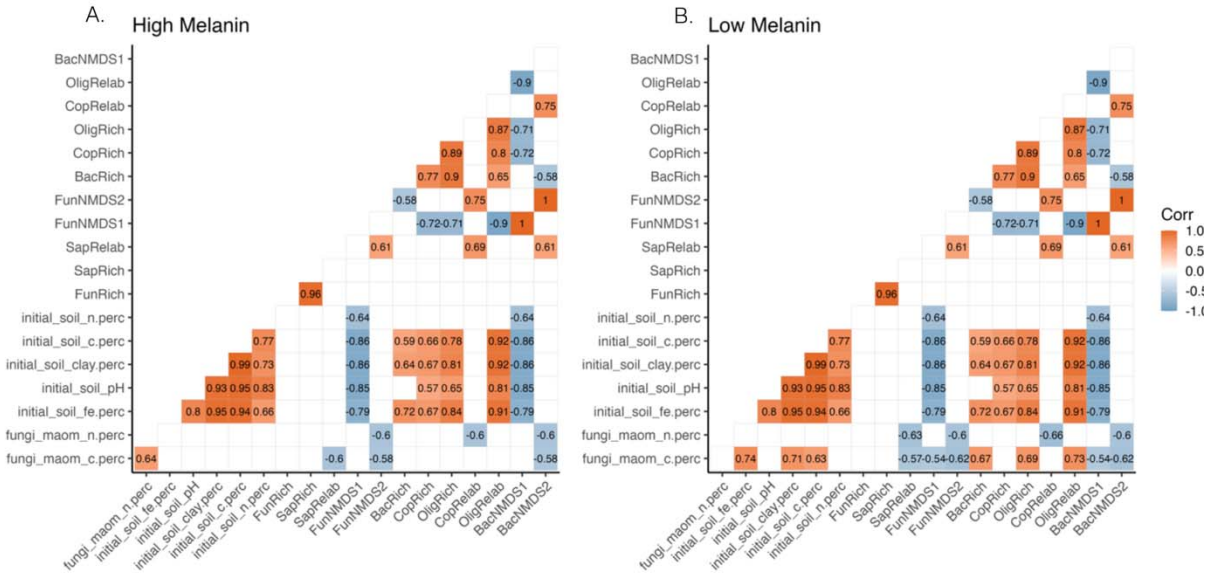

Figure S3. Pearson's correlation matrix and coefficients (r) for relationships among initial soil properties for soils amended with A. high melanin and B. low melanin necromass. Non-significant correlations (P > 0.05) are represented by white squares. Soil properties include pH, clay, carbon and nitrogen concentrations, bacterial community composition (NMDS1 and NMDS2 scores), bacterial oligotroph and copiotroph relative abundance and fungal saprotroph relative abundance.

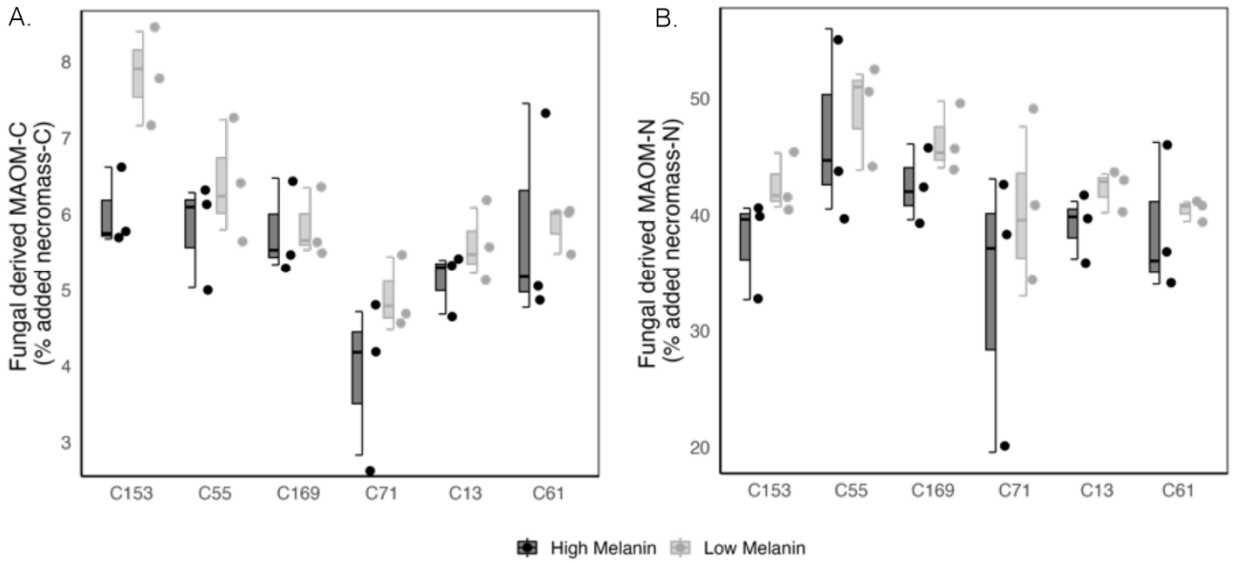

Figure S4. Box and whisker plots of fungal necromass derived mineral associated organic matter (MAOM) carbon (C) and nitrogen (N) formation for the different sites. Dark gray boxes and points represent high melanin (HM) necromass and light gray boxes and points represent low melanin (LM) necromass.

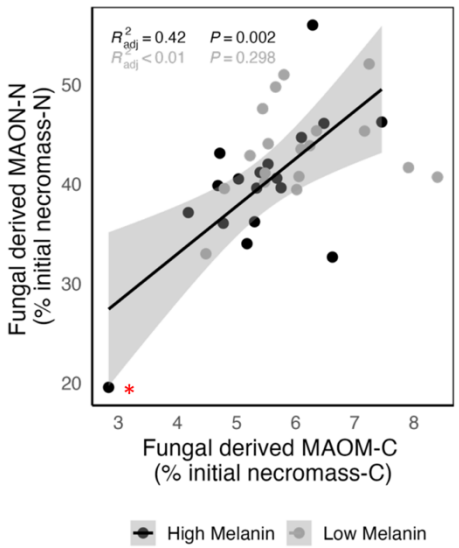

Figure S5. Linear regression of fungal necromass derived mineral associated organic matter (MAOM) carbon (C) and nitrogen (N) formation. The relationship is only significant for low melanin necromass. When the point next to the red Asterix is removed the relationship is no longer significant (R2 = 0.13, p = 0.09).

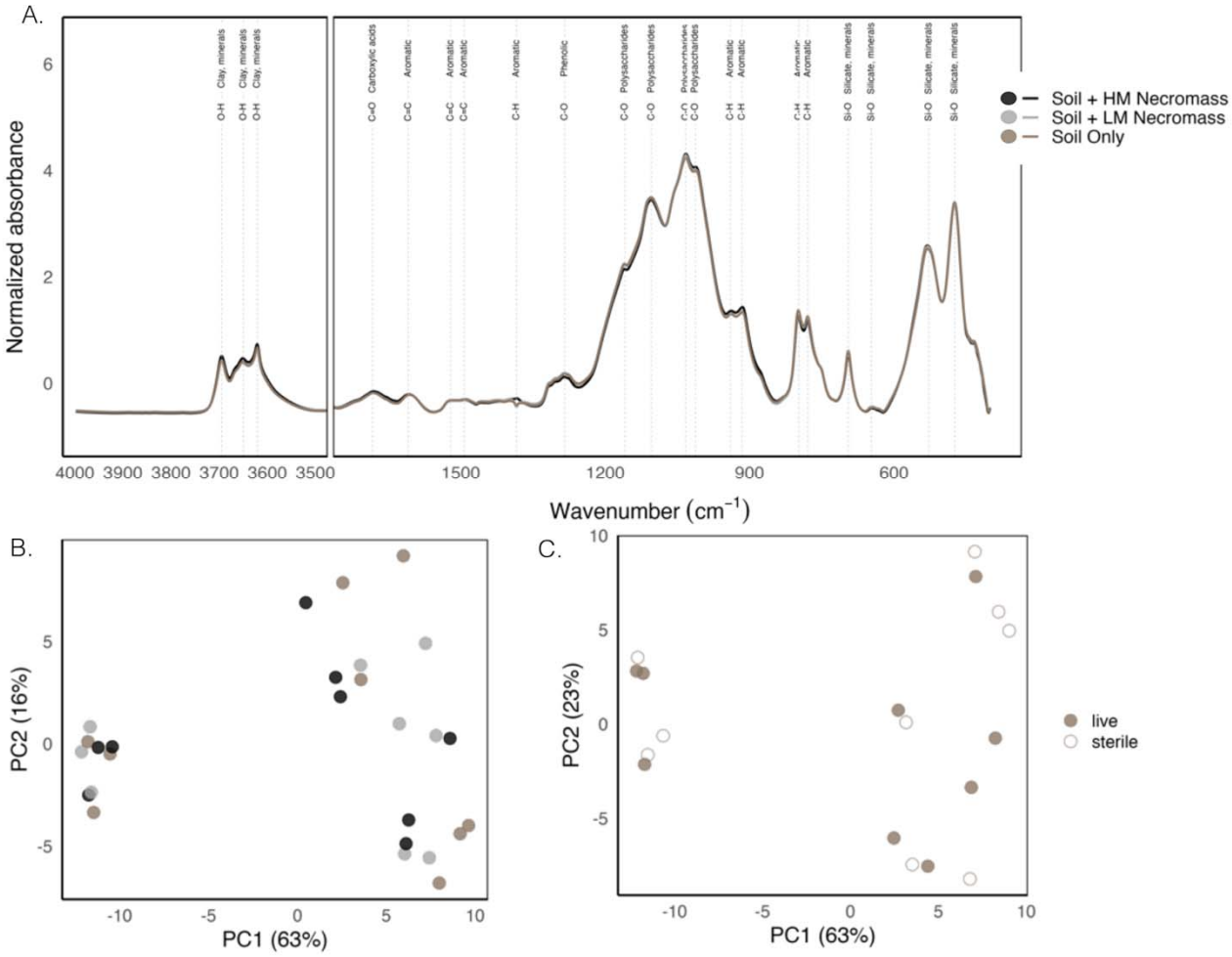

Figure S6. A. Diffuse Reflectance Infrared Fourier transform spectroscopy (DRIFTS) spectra with annotated peaks for MAOM samples grouped by necromass treatment. Principal Component Analysis (PCA) biplots of DRIFT spectra for mineral associated organic matter (MAOM) samples from microcosms colored by B. necromass treatment and C. sterilization treatment.

A.

Peak ID	Wavenumber	Functional group	Potential Compound
1	2955.7 (2945-2965)	C-H	Aliphatic
2	2925.81 (2915-2935)	C-H	Aliphatic
3	2853.48 (2843-2863)	C-H	Aliphatic
4	1709.77 (1699-1719)	C=O	Carbonyl
5	1649.02 (2915-2935)	C=O	Amide I*
6	1546.8 (1701-1598)	N-H	Amide II*
7	1453.26 (1443-1463)	C-H	Aliphatic
8	1398.29 (1388-1408)	C-H	Aliphatic
9	1248.82 (1238-1258)*	C-O	Aromatic*
10	1108.99 (1098-1118)	C-O	Polysaccharide
11	1040.52 (1030-1050)	C-O	Polysaccharide
12	1017.38 (1007-1027)	C-O	Polysaccharide
13	938.3 (928-948)	C-H	Alkenes

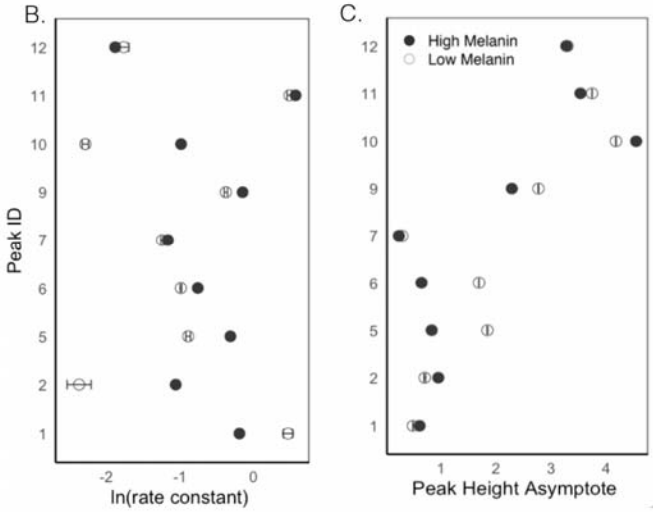

Figure S7. A. Peak annotations for SIPT spectra B. Rate constants and C. Asymptotic peak heights generated from asymptotic regression models. White rows represent Peak IDs for which we were unable to fit an asymptotic regression model. *Peak 5 is mainly attributed to C=O stretching of Amide I, and partially attributed to C-N stretching and N-H bending. While peak 6 is mainly attributed to N-H bending and partially to C-N stretching. Peak 9 at 1248 cm^{-1} and the shoulder 1230 cm^{-1} might also attributed to PO2- asymmetric stretching (Stuart 2004).